The Speed of Observed and Theoretical Long Extratropical Planetary Waves

PETER D. KILLWORTH

Southampton Oceanography Centre, Southampton, United Kingdom

DUDLEY B. CHELTON AND ROLAND A. DE SZOEKE

College of Oceanic and Atmospheric Sciences, Oregon State University, Corvallis, Oregon

(Manuscript received 19 August 1996, in final form 12 February 1997)

ABSTRACT

Planetary or Rossby waves are the predominant way in which the ocean adjusts on long (year to decade) timescales. The motion of long planetary waves is westward, at speeds ≥ 1 cm s^{-1}. Until recently, very few experimental investigations of such waves were possible because of scarce data. The advent of satellite altimetry has changed the situation considerably. Curiously, the speeds of planetary waves observed by TOPEX/Poseidon are mainly faster than those given by standard linear theory. This paper examines why this should be. It is argued that the major changes to the unperturbed wave speed will be caused by the presence of baroclinic east–west mean flows, which modify the potential vorticity gradient. Long linear perturbations to such flow satisfy a simple eigenvalue problem (related directly to standard quasigeostrophic theory). Solutions are mostly real, though a few are complex. In simple situations approximate solutions can be obtained analytically. Using archive data, the global problem is treated. Phase speeds similar to those observed are found in most areas, although in the Southern Hemisphere an underestimate of speed by the theory remains. Thus, the presence of baroclinic mean flow is sufficient to account for the majority of the observed speeds. It is shown that phase speed changes are produced mainly by (vertical) mode-2 east–west velocities, with mode-1 having little or no effect. Inclusion of the mean barotropic flow from a global eddy-admitting model makes only a small modification to the fit with observations; whether the fit is improved is equivocal.

1. Introduction

Planetary, or Rossby, waves play a fundamental part in the spinup of the ocean, the maintenance of western boundary layers, and many other features. They owe their existence to variation in the Coriolis parameter, which permits propagation along great-circle waveguides in a westward sense. Unlike rapid coastal Kelvin waves, planetary waves move slowly, at typical speeds of a few centimeters per second. Location of such waves in patchy temperature data required careful attention (White 1977, 1985; Kessler 1990), and oceanographers have been in the curious position for the most part in having a theory before it could receive unequivocal confirmation.

The theory for such waves is well known (Dickinson 1978; Gill 1982; LeBlond and Mysak 1978) and holds for an ocean whose background state is at rest, with a uniform depth. The linearized three-dimensional equations are cast onto an infinite, complete set of vertical normal modes. For each mode, the resulting free horizontal (i.e., two-dimensional) problem, with an equivalent depth and reduced gravity, can be solved. All phase speeds are westward, and waves that are long in all directions are nondispersive. The lowest-order mode (zeroth) is barotropic, and almost uniform vertically for a free surface; with a rigid lid the mode is completely uniform vertically. Its phase speed is rapid, probably unobservable by altimetry (Chelton and Schlax 1996, hereafter CS) and will not concern us.

The remaining modes are baroclinic, and have phase speeds of order a few centimeters per second. The phase speeds depend inversely on the square of the Coriolis parameter, and waves take only months to cross an ocean basin at low latitudes, and years to decades at higher latitudes. The vertical structure of these waves becomes progressively more complicated as the mode number increases, while the phase speed decreases. Attention has thus tended to concentrate on the first mode, in which the horizontal velocity has one sign change in the vertical.

Since the speeds of these modes are straightforward to compute—only the background stratification is required for their determination—theoreticians have waited with interest for sufficient satellite altimetric data to demonstrate the existence and nature of planetary

Corresponding author address: Dr. Peter D. Killworth, Southampton Oceanography Centre, Empress Dock, Southampton SO14 3ZH, United Kingdom.
E-mail: p.killworth@soc.soton.ac.uk

waves. Several recent papers (Le Traon and Minster 1993; CS; Rogel et al. 1997, submitted to *J. Geophys. Res.*, hereafter RMBMV; Cipollini et al. 1996, 1997; Glazman et al. 1996) present such data. They find clear evidence of westward propagation of long waves throughout the area of ocean surveyed by TOPEX/Poseidon. Surprisingly, away from the Tropics the westward phase velocity shows values inconsistent with theory. Estimates vary slightly between authors, depending on the method used and the precise region analyzed, but the estimates are generally consistent. In the range 10° to 20° (N and S), there is much scatter, but observed values between 1 and 1.5 times the theoretical value are found. Poleward of 20° the ratio of observed to theoretical rises rapidly, reaching 2 at about 30° in both hemispheres, and farther poleward the ratio remains consistently around twice the theoretical value. The waves observed are all *long*, with wavelengths of order 300 to 500 km or more. [Jacobs et al. (1994) also found evidence of such waves in the North Pacific from both *Geosat/ERS-1* and TOPEX/Poseidon data, with westward speeds of 4.9 cm s^{-1} at 30°N; they felt that such wave speeds fitted linear theory, whereas the calculations here and by CS would indicate speeds from 2.7 cm s^{-1} in the eastern Pacific to 3.8 cm s^{-1} in the west from standard theory.]

Some care with interpretation is necessary: RMBMV (1997) observe some eastward propagating signals, which they take to be Gulf Stream meanders, as well as some rapid westward propagation in the western North Atlantic, which they ascribe to Gulf Stream rings. Thus, not all the phenomena are, or need necessarily be, planetary waves.

Another difficulty is that most authors have examined the data solely for east–west propagation, rather than for a general orientation. The angle of propagation is irrelevant for linear long planetary waves, since the speed at which crests move westward is independent of the orientation of the wave. Although Le Traon and Minster (1993) observed southwest propagation in the South Atlantic, Forbes et al. (1993) analyzed crossovers from *Geosat* data in the South Atlantic and found propagation within at most 5° of absolute westward. Cipollini (personal communication, 1997) has found only occasional evidence of any north–south propagation in the TOPEX/Poseidon data. Thus to a first approximation, only westward propagation need be considered.

Figure 1a, redrawn from CS, summarizes the difficulty. Phase speeds are, simply, faster than linear theory predicts, and CS were forced to conclude that ''the standard theory for freely propagating, linear, baroclinic Rossby waves is deficient in predicting the observed phase speeds.'' How can this be? Linear theory, whatever its shortcomings, has proven most valuable in interpreting other oceanic features. Clearly one or more of the assumptions inherent in linear theory has broken down. Possible candidates are

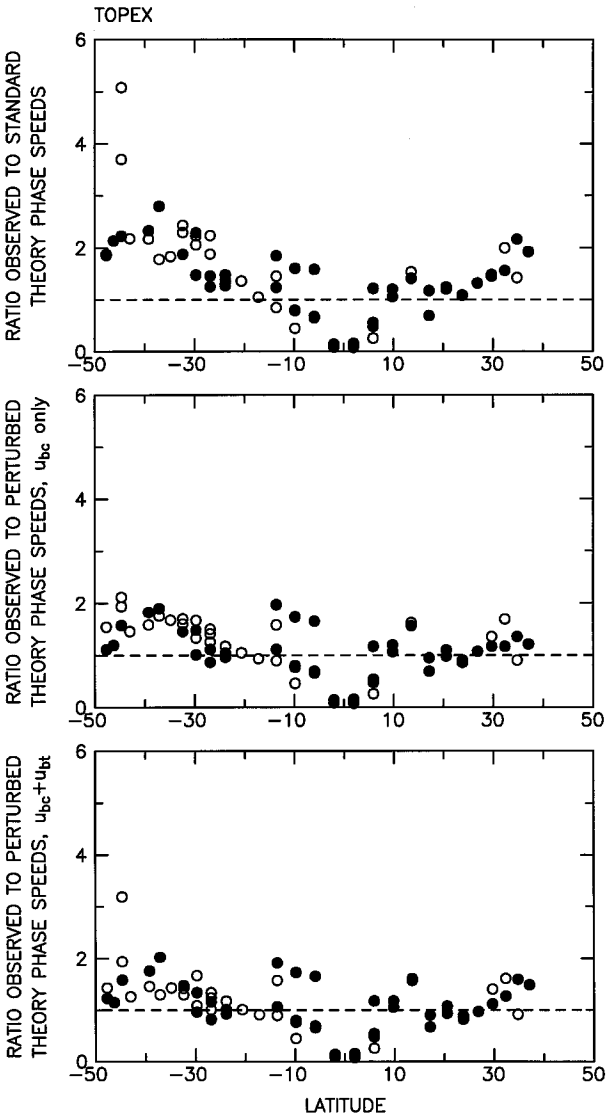

FIG. 1. Ratio of observed (TOPEX/Poseidon) to predicted long linear planetary wave speeds, as a function of latitude. Black circles show data from Pacific estimates, open circles from Atlantic and Indian Ocean estimates: (a) standard theory, (b) the theory in this paper including a baroclinic mean east–west velocity, and (c) including the additional effect of the barotropic east–west velocity. Minor differences between (a) and that in CS are due to later refinement of the TOPEX data.

1) the flow is forced (by wind and/or buoyancy) and is part of the coupled system, so is not free;
2) the ocean has a varying bottom;
3) the response is fundamentally nonlinear;
4) the background state of the ocean is not at rest.

We examine these in turn; further discussions can be found in the observations cited.

1) Forcing of the ocean at its surface can induce resonances (White 1977; Meyers 1979). The precise form of the response depends on the eastern boundary conditions, but under some circumstances the forced re-

sponse appears to have a phase speed double that of the original wave. However, it is hard to see how precise resonances can occur so ubiquitously to generate such a uniform overestimate of phase speed. Coupling with the atmosphere in equatorial regions affects wave speeds, though this is less likely to occur at midlatitudes.

2) Topographic effects occur throughout the ocean, though in a manner far from understood (even such a basic concept as topographic steering has proved hard to quantify and describe). A bottom slope can modify the speed of a planetary wave (Rhines 1970), but again it would be hard to imagine bottom slopes always aligned precisely to speed up the planetary waves. Direct modal interactions (Anderson and Killworth 1977) are mainly the modification of the barotropic mode by the first baroclinic, with little reverse effect.

3) It is possible that the waves have sufficient amplitude to induce nonlinear aspects to play a role. The largest such manifestation is likely to be in the planetary geostrophic regime (i.e., the flow remains geostrophic to leading order but nonlinearity is felt in the conservation of buoyancy). This was explored by Anderson and Killworth (1979) and adapted for the Antarctic Circumpolar Current by Clarke (1982). The wave can now alter the local stratification, and its local phase speed is precisely that of a linear wave with that (revised) stratification. It thus seems implausible that waves faster than linear are so common, while the vertical structures necessary to support such speeds are not observed. Indeed, Chelton et al.'s (1997, hereafter CDSNS) analysis of deformation radii shows little seasonal variation.

We are thus led to examine option 4, that is, that the background ocean is not in a state of rest [discussed previously by Herrmann and Krauss (1989) and alluded to by most authors (cf. Dickinson 1978)]. In terms of inertia–gravity modes, whose phase speeds are a few meters per second, a state of rest is clearly a good approximation save in energetic regions such as western boundary layers or fronts. However, phase speeds of planetary waves are of the same magnitude as mean flows and so might well be modified by them.

The ideal case for solution would be time- and space-varying propagation through mean flow with general orientation. Such a problem is difficult to analyze—it is, indeed, one of the basic issues in physical oceanography. In very simple layered models where the number of layers is small (one or two), characteristic methods can be employed. [In the case of one active layer the mean flow has no direct effect save through the modification of local phase speed by variation of local depth, a case considered by Anderson and Killworth (1979).] For more layers, and for continuous stratification, such methods fail save in special cases. Thus the simpler problem presents itself: evaluation of the *local* phase speed in a mean flow with general orientation.

This problem, too, remains difficult on several grounds. North–south mean flow, together with vortex stretching, implies the existence of mean vertical velocities, adding considerably to the complexity (unless the mean forcing, which is required to maintain a north–south flow, is also assumed to exactly cancel the vortex stretching terms and leave purely horizontal parallel flow).[1] However, if we restrict attention to waves whose direction of propagation is purely east–west, this is not a problem, and, as we shall show, any mean north–south flow has no effect on the solution. (More general directions of propagation will be discussed briefly later.)

For the most part, then, we shall consider only east–west mean flows henceforth. The most trivial case would be a depth-independent westward mean flow, which would simply Doppler-shift the planetary wave. But in much of the ocean, changes in phase speeds, at least on a global average, of more than some few millimeters per second would be hard to achieve by this mechanism. (This may well have a role to play at high latitudes where planetary wave speeds are small, however.) This implies that the much harder case of a baroclinic mean flow must also be examined. We shall, indeed, usually assume that the mean flow has no vertical integral and consider the Doppler-shift issue again later using numerical model output.

Inclusion of a baroclinic mean flow, which changes the local potential vorticity gradient, in a wave problem raises many issues. Chief among them are the drastic reduction to a finite number of modes (Killworth and Anderson 1977; Pedlosky 1964), the prospect of baroclinic instability (Gill et al. 1974; Killworth and Anderson 1977; Pedlosky 1987), and the suppression or modification of short waves by critical layers (Killworth 1979). The necessary conditions for instability are frequently satisfied, often because the β term is modified by vertical shear and/or topography to an ''effective β,'' which can take both signs. (We might thus wonder whether such an effective β could be sufficiently larger than the planetary term to explain the increase in phase speed; but see below.) However, many of the realistic profiles considered by Gill et al. (1974) were stable. Curiously, although linear instability theory is well developed, it has not been applied systematically to ''typical'' mean flows until recently, in attempts to compare the eddy fields from eddy-admitting GCMs with local flow properties (Beckmann et al. 1994).

If we restrict attention to long waves, the problem simplifies conceptually. Clearly growth rates, which are $k\mathrm{Im}(c)$, where k is a wavenumber and c the complex phase speed, becomes very small; this is evident in Killworth and Anderson (1977), for example. As a typical example, if k is $2\pi/500$ km, and $\mathrm{Im}(c)$ is 0.1 cm s^{-1}, the wave has an e-folding time of 3 years [such values for $\mathrm{Im}(c)$ are realistic, as will be shown later]. With any

[1] This awkwardness is almost invariably ignored in the few studies of perturbations to nonzonally oriented mean flow extant in the literature.

plausible dissipation, such tiny growth is unlikely to be observed.

Of course, weak growth rate at low wavenumber does not imply that the flow cannot support active instabilities at finite wavenumber; in general it can and will. But these are preferentially of wavelength of order the deformation radius, say 30–100 km (Killworth 1980), whereas the planetary waves observed by CS are far longer. Eddies on small scales can thus grow, but are not what is being observed, or studied, here.

This leads us to consider the simplest long-wave problem, which may or may not have complex solutions (we will see that in most cases of interest the solutions are real, in fact). We shall examine waves in the presence of an east–west mean flow, with a corresponding north–south density gradient.

In section 2 we set up the problem and show that a degree of degeneracy exists, in the sense that an arbitrary multiple of the wave mode solution can be added to the mean flow without altering the solution. Thus the presence of first baroclinic mode mean flow can, in some sense, be expected to have little effect on the propagation of the first mode; this will turn out to be generally true. It is the second and higher baroclinic modes that modify the westward phase speed of the first baroclinic mode. In section 3 we find approximate solutions for the eigenvalue problem when the mean flow is small, of the same order as, and larger than, the fastest linear planetary mode. There is almost always a solution whose phase velocity is approximately the minimum mean velocity plus the mode 1 planetary wave velocity. Phase speeds twice the unperturbed speed are attained at higher latitudes. Section 4 compares these predictions with numerical solutions for the case of uniform stratification and, more realistically, stratification decaying exponentially with depth. In section 5 we compute the local solutions in the World Ocean and show that ratios similar to those observed, though slightly smaller, are found using this mechanism. Section 6 gives an approximate explanation for the findings, and section 7 discusses the effect of the mean barotropic east–west flow.

2. The eigenvalue problem

It is useful to first recall linear normal mode theory. We follow Gill (1982). The ith linear normal mode satisfies the vertical Sturm–Liouville problem

$$\hat{h}_{izz} + \frac{N^2}{C_i^2}\hat{h}_i = 0, \tag{1}$$

where z denotes the vertical, $\hat{h}_i$ is the vertical structure (corresponding to the vertical velocity), $N(z)$ is the buoyancy frequency given by $N^2 = -g\rho_z/\rho_0$ (g is acceleration due to gravity, ρ the density, and ρ_0 the reference density), and C_i the phase speed of long gravity waves. Here, $\hat{h}_i$ vanishes at the surface ($z = 0$) and floor ($z = -H$). The modes are assumed arranged in decreasing order of C_i. The higher modes have $C_i \propto i^{-1}$ by WKBJ theory (cf. CDSNS).

For convenience we shall nondimensionalize, scaling z on H, N on some typical N_0, and C_i on N_0H. The resulting equation is of identical form. The equivalent of (1) for horizontal velocity structure $\hat{u}_i(z)$ is given by

$$\hat{u}_i = C_i^2\hat{h}_{iz} \tag{2}$$

so that $\hat{u}_i$ satisfies its own Sturm–Liouville problem

$$\left(\frac{\hat{u}_{iz}}{N^2}\right)_z + \frac{\hat{u}_i}{C_i^2} = 0; \qquad \hat{u}_{iz} = 0, \qquad z = 0, -1, \tag{3}$$

which is again of the same form dimensionally. The $\hat{h}_i$ or the $\hat{u}_i$ form a complete set, and we shall use the normalization

$$\int_{-1}^{0} N^2\hat{h}_i\hat{h}_j\, dz = \delta_{ij}.$$

The long planetary wave problem can be tackled in two ways. The simplest is by using Welander's (1959) M notation. We write (dimensionally for the moment)

$$M_z = \frac{p}{\rho_0}; \qquad M_{zz} = -\frac{g\rho}{\rho_0}; \qquad u = -\frac{M_{zy}}{f};$$

$$v = \frac{M_{zx}}{f}; \qquad w = \frac{\beta}{f^2}M_x, \tag{4}$$

where f, β are the Coriolis parameter and its northward derivative.

Although we shall deal for the most part with perturbations to an east–west mean flow, we initially linearize the equation for conservation of density about a mean state $u(x, y, z)$, $v(x, y, z)$, $\rho(x, y, z)$ in thermal wind balance. We assume there to be no mean vertical velocity. [The vortex stretching implicit in (4), which would imply a mean vertical velocity when there is north–south flow, must be balanced by some complicated mean forcing, which we discuss no further. This is standard in linear perturbation theory.] Then, using primes to denote small perturbations:

$$\rho'_t + u\rho'_x + u'\rho_x + v\rho'_y + v'\rho_y + w'\rho_z = 0, \tag{5}$$

we seek a solution varying as fn$(x\cos\theta + y\sin\theta - ct)$, for some angle of propagation θ. This is essentially a slowly varying solution so that $c = c(x, y)$ parametrically. The speed at which crests would appear to move westward in (5) is $dx/dt = c/\cos\theta \equiv c_w$. Substituting into (5) gives, setting $\tilde{u} = u + v\tan\theta$,

$$(\tilde{u} - c_w)W_{zz} - \tilde{u}_z W_z + \frac{\beta N^2}{f^2}W = 0, \tag{6}$$

where W denotes the perturbation to M (the notation being chosen since W plays the role of the vertical velocity eigenvector). Immediately a difficulty about near-northward propagation appears. If θ is nearly $\pi/2$, and $v \neq 0$, $\tilde{u}$ can be as large as we like, dominating the β

term. Under some circumstances (a solution with similar mathematics is presented later), c_w can also be as large as desired.

To avoid these difficulties, we shall restrict attention to east–west propagation (but will return to this aspect later). Setting $\theta = 0$, the terms involving v disappear identically, and (6) simplifies to

$$(u - c)W_{zz} - u_z W_z + \frac{\beta N^2}{f^2} W = 0. \tag{7}$$

This equation will be used henceforth.

An alternative approach would be from standard quasigeostrophic theory (Pedlosky 1987). If we write $P = W_z$ in (7), we have

$$(u - c)\left(\frac{f^2}{N^2}P_z\right)_z + \left[\beta - \left(\frac{f^2}{N^2}u_z\right)_z\right]P = 0, \tag{8}$$

which is the usual streamfunction equation with wavenumber k set to zero.

We now nondimensionalize (7). The velocity u and unknown phase speed c are nondimensionalized on $\beta N_0^2 H^2/f^2$ (note that the internal wave speeds C_i are nondimensionalized on the much larger value $N_0 H$), giving an eigenvalue problem

$$(u - c)W_{zz} - u_z W_z + N^2 W = 0 \tag{9}$$

with boundary conditions

$$W = 0, \qquad z = 0, -1. \tag{10}$$

In the case when u vanishes, (9) becomes

$$-c_i W_{zz} + N^2 W = 0, \tag{11}$$

which is of the form (1), with the correct identification that

$$c\ (=c_i) = -C_i^2 \tag{12}$$

for the ith planetary mode (i.e., dimensionally $c = -\beta C_i^2/f^2$). The ith planetary mode, for large i, has speed c proportional to i^{-2}. The fastest, and the mode we shall predominantly be interested in, is the first mode.

If c is real, then (9) can possess a critical layer (where $u = c$). At such a point, there are two solutions. One is well behaved, the other has a logarithmic second derivative. In general, the well-behaved solution alone cannot satisfy both boundary conditions (10). Indeed, even if the local northward gradient of potential vorticity $q_y = \beta - [(f^2/N^2)u_z]_z$ vanishes at such a point [cf. discussions in Pedlosky (1989) and earlier references therein], which gives two well-behaved independent solutions instead of one, the problem is homogeneous and so still cannot in general be solved (though special cases can be constructed, for example, with finite depth ranges where q_y vanishes). Thus if we begin with a solution that has no critical layer (e.g., zero u) and vary u gradually in such a way that the existence of a critical layer approaches, the phase velocity and eigenmode can be expected to become complex.

Few of the known results from baroclinic instability theory (Pedlosky 1987) are useful here; the semicircle theorem, for example, adjusted to include the baroclinic deformation radius, gives weak bounds in the zero wavenumber limit. From the above discussion, we can show that (except for special cases) for real solutions,

$$c < u_{\min} < 0,$$

where $u_{\min}$ is the least (i.e., most westward) value of u. Thus real solutions propagate westward at a rate that is at least $u_{\min}$, so that regions where this is large might be expected to have faster westward propagation (assuming the solution remains real). It is straightforward to show that for complex solutions,

$$\mathrm{Re}(c) < u_{\max},$$

where the notation is obvious; but since the maximum u field is positive, by supposition, this is of little help.

The necessary conditions for instability (Charney and Stern 1962) continue to hold in the long-wave limit, of course. These depend on the northward gradient of potential vorticity (also known as the effective β), q_y, defined above. Instability can only occur if one or more of the following holds: q_y changes sign in the interior; $q_y u_z < 0$ at the surface; or $q_y u_z > 0$ at the floor. However, even if the necessary conditions are satisfied, either the (possibly unique) or the fastest westward solution can still be real.

Before proceeding, we may note one immediate result from (9) that applies only in the long-wave limit. Providing the eigenmode is real, adding an arbitrary multiple of W_z (or P) to u does not change the eigenmode at all [the terms cancel in (9) identically]. In particular, the *addition of any amount* of the mode 1 u field does not alter the *westward propagation* of the mode 1 eigenfunction in any way. This result has appeared in various guises in the literature (e.g., Schopf et al. 1981; Meyers 1979; Herrmann and Krauss 1989) but is seen most simply and generally by use of (9). Note that a one-layer reduced gravity model automatically possesses only mode 1 fields, so that this finding applies to all such models. This explains the findings of the ''non-Doppler effect'' of Held (1983), as well as those of Chang and Philander (1989) and Kessler (1990). Thus, in some sense, if the mode $W(z)$ is ''near'' the first internal mode, say, then the effect of an applied u field, which is also ''near'' the first mode, can be expected to be very small. We will quantify this in the next section.

3. Approximate solutions

There are few approximate results, and almost no exact solutions, for baroclinic instability problems. Although we are primarily interested here in real solutions (i.e., simple propagating waves), there is little background to draw on. However, before solving the problem numerically, it is of interest to explore some approximate methods. We shall solve the problem, successively,

for cases in which the mean flow is (a) small, (b) of the same order as, and (c) much larger than the mode 1 westward phase speed.

a. Small amplitude velocity

We first examine the effects of a small u field, where "small" denotes $u \ll |c_i|$ for some mode i. Note that for any finite u there will be an infinite number of (unperturbed) normal modes for which u exceeds the size of the mode speed, by the WKBJ results mentioned above. We must therefore consider a low-order mode for the approximation to be valid and, in fact, will normally consider mode 1. Take a basic solution (11) denoted by a suffix 0; that is,

$$-c_i W_{0zz} + N^2 W_0 = 0. \tag{13}$$

Now pose

$$W = W_0 + u_0 W_1; \qquad c = c_i + u_0 c_{i1}; \qquad u = u_0 \hat{u}(z), \tag{14}$$

where $\hat{u}(z)$ is of order 1 and u_0 is its amplitude, assumed small. Substituting in (9) gives

$$-c_i W_{1zz} + N^2 W_1 = -(\hat{u} - c_{i1}) W_{0zz} + \hat{u}_z W_{0z}. \tag{15}$$

Now (13) times W_1 minus (15) times W_0, and integration, gives after a little algebra

$$c_{i1} \int_{-1}^{0} N^2 W_0^2 \, dz = \int_{-1}^{0} N^2 \hat{u} W_0^2 \, dz - c_i \int_{-1}^{0} \hat{u}_z W_{0z} W_0 \, dz. \tag{16}$$

If W_0 is identically $\hat{h}_i$ (as it can be without loss of generality), then the integral on the lhs is unity, and the correction c_{i1} to the phase speed is given by the difference between two integrals, which can be trivially computed. This formula is generated more generally by the truncation method to be discussed next. If W_0 is indeed mode 1 in shape, then for typical ocean values the sign of the rhs is dominated by that of the first term, and has the sign of u at mid-depth. Thus when u is westward (eastward) at mid-depth, the correction c_{i1} is also westward (eastward).[2]

In the first case, this makes the phase speed more westward and, so in general, can drive the solution away from possible critical layer behavior if the decrease in phase speed is fast enough to counter the approach of the critical layer as u_0 increases. In the second case, the solution is moved toward complex modes and eventually the approximation would break down.

Other solutions can, of course, be present, although these are usually few in number; typically the solution above has the fastest westward propagation.

b. u of the same order as c_1; casting onto linear normal modes

The simple approximation above implicitly assumed that the solution was well described by a single linear mode (the one being linearized about). When u is larger, this is not necessarily the case (although the solution normally remains close to mode 1 in shape, as we shall see). We can instead cast the solution onto many or all of the linear modes. We consider u and the response W as a sum of normal modes, and write

$$u = \sum_{i=1}^{\infty} u_i \hat{u}_i(z); \qquad W = \sum_{j=1}^{\infty} W_j \hat{h}_j(z) \tag{17}$$

and substitute into (9):

$$\sum_{i=1}^{\infty}\sum_{j=1}^{\infty} u_i W_j \hat{u}_i \hat{h}_{jzz} - c \sum_{j=1}^{\infty} W_j \hat{h}_{jzz} - \sum_{i=1}^{\infty}\sum_{j=1}^{\infty} u_i W_j \hat{u}_{iz} \hat{h}_{jz} + N^2 \sum_{j=1}^{\infty} W_j \hat{h}_j = 0. \tag{18}$$

Multiplying by $\hat{h}_k$, integrating over depth, and use of (1), (3), and (4) gives

$$\sum_{i=1}^{\infty}\sum_{j=1}^{\infty} u_i W_j \left(-\alpha_{ijk}\frac{c_i}{c_j} + \alpha_{jik}\right) + \left(1 - \frac{c}{c_k}\right) W_k = 0, \tag{19}$$

where c_i are the unperturbed planetary wave speeds and the α_{ijk} are triple integrals of the unperturbed normal modes

$$\alpha_{ijk} = \alpha_{ikj} = \int_{-1}^{0} N^2 \hat{h}_{iz} \hat{h}_j \hat{h}_k \, dz. \tag{20}$$

Note that in the double sum in (19), the contributions when $i = j$ cancel identically, a further ramification of the noninteraction result above.

The set (19) forms an infinite matrix eigenvalue problem of the form $\mathbf{A}W = cW$. For simplicity, suppose that u has only one modal component, mode R, say. Since there is no direct contribution from the mode R–mode R interaction, and mode 1 can be expected to remain the fastest, we assume that $R \neq 1$ (later computations will show that the inclusion of mode 1 into the u field indeed has little effect on the phase speed).

We now truncate the representation of W to two terms (to be extended below): W is cast onto modes 1 and R. The system (19) reduces to two equations:

$$W_1\left(1 - \frac{c}{c_1}\right) + u_R W_1\left(-\alpha_{R11}\frac{c_R}{c_1} + \alpha_{1R1}\right) = 0$$

$$W_R\left(1 - \frac{c}{c_R}\right) + u_R W_1\left(-\alpha_{R1R}\frac{c_R}{c_1} + \alpha_{1RR}\right) = 0. \tag{21}$$

[2] The situation is not always so clear. If N is constant, and $u \propto (z + \tfrac{1}{2})$, both terms on the rhs of (16) cancel by symmetry and the expansion would fail.

The first of (21) gives a linear equation for c; the second defines the relative amplitude of W_R and W_1 and does not concern us. Then c is given by the approximate form

$$c = c_1 + u_R(-\alpha_{R11}c_R + \alpha_{1R1}c_1). \tag{22}$$

This is precisely the same as (16), as a little substitution will show. Thus to this degree of approximation c varies linearly with the amplitude of the u mode applied. If this amplitude has one sign, which depends on the sign of the bracket in (22), c will become more westward than c_1, avoiding a critical layer if the dependence on u_R is strong enough. If the amplitude of u has the opposite sign, at some amplitude a critical layer will occur and the approximation will break down.

It will turn out that this approximation is frequently quite accurate. A better approximation can be made by extending the modes that W is cast onto. For simplicity in presentation only, assume $R = 2$ and cast W onto modes 1, 2, and 3. Then (19) yields three equations. Of these, the second is the only one to contain W_2, and so defines its size (the noninteraction result applying again). The first and third equations then yield

$$\underbrace{u_2W_1\left(-\alpha_{211}\frac{c_2}{c_1} + \alpha_{121}\right)}_{A} + \underbrace{u_2W_3\left(-\alpha_{231}\frac{c_2}{c_3} + \alpha_{321}\right)}_{B} + W_1\left(1 - \frac{c}{c_1}\right) = 0 \tag{23}$$

$$\underbrace{u_2W_1\left(-\alpha_{213}\frac{c_2}{c_1} + \alpha_{123}\right)}_{C} + \underbrace{u_2W_3\left(-\alpha_{233}\frac{c_2}{c_3} + \alpha_{323}\right)}_{D} + W_3\left(1 - \frac{c}{c_3}\right) = 0. \tag{24}$$

The resulting quadratic (labeling the brackets as indicated) is

$$c^2 - c[c_1 + c_3 + u_2(Ac_1 + Dc_3)] + c_1c_3[1 + (A + D)u_2 + u_2^2(AD - BC)] = 0, \tag{25}$$

which is of the form

$$c^2 + c(R_1 + R_2u_2) + R_3(1 + R_4u_2 + R_5u_2^2) = 0, \tag{26}$$

where all the coefficients are known. This may yield real or complex values dependent upon the values of the R_j.

When u does not resemble a single mode, this approach becomes less useful. If u is cast onto a collection of modes and then characterized by an overall amplitude, one would need to cast W onto many modes, resulting in intractable equations; little can be said.

Note finally that (26) would imply that as $|u_2|$ becomes large, c takes the same value whether u_2 is positive or negative. Save in certain cases of symmetry this cannot occur so that (26) must eventually fail as the amplitude of the flow increases. The following method can then be used.

c. *u much larger than c_1*

The final case that can be analyzed is not very physical but is included because the solution can be found explicitly and gives a useful guide to the total behavior of the system. We now pose $u = u_0\hat{u}(z)$, where the amplitude $u_0 > 0$ is large, and $\hat{u}(z)$ is assumed to be of order 1. This gives the natural expansion

$$c = u_0\hat{c}_0 + \hat{c}_1 + \cdots, \tag{27}$$

where $\hat{c}_0$ is of order 1 and the size of $\hat{c}_1$, though much smaller, is not yet obvious. We consider possible values for $\hat{c}_0$ first, assuming c to be positive. To leading order the first two terms in (9) are $O(u_0)$, while the third is $O(1)$, so that (9) is simply

$$(u - \hat{c}_0)W_{zz} - u_zW_z = 0. \tag{28}$$

If $(u - \hat{c}_0)$ never vanishes (i.e., is everywhere positive), then (28) would have the integral

$$W_z = A(u - \hat{c}_0),$$

which upon integration and application of the boundary conditions yields no solution: clearly W_z must take both signs if W is to vanish top and bottom. It therefore follows that $(u - \hat{c}_0)$ vanishes somewhere. If this occurs at a true zero (i.e., $u - \hat{c}_0$ takes both signs), then (28) is singular, there is a true critical layer and c becomes complex. The only way to avoid this is if $(u - \hat{c}_0)$ reaches zero only quadratically, so that $(u - \hat{c}_0) \geq 0$.

In this case, clearly $\hat{c}_0 = u_{\min}$, where $u_{\min}$ is the least value attained by the u distribution.[3] Now $u = u_{\min}$ at one, or possibly more, values of z in one of several ways. There may be an (least) extremum at the surface or floor. The special case of a minimum precisely at surface or floor could occur. Finally, there may be a true minimum at mid depth. Only this final case appears to have a solution.

We assume that $u_{\min}$ is attained at mid depth, at $z = z_0$, say. (If there is more than one such location, the proof is only marginally altered.) Near $z = z_0$, then, (28) breaks down and there is a thin interior boundary layer of thickness $u_0^{-2/3}$ in which the correction $\hat{c}_1$, which turns out to be of order $u_0^{1/3}$, becomes important. In this, writing $u_{zz} = u_{zz}(z_0) > 0$, $u - \hat{c}_0 - \hat{c}_1$ is approximately $\frac{1}{2}u_{zz}(z - z_0)^2 - \hat{c}_1$. Since we need $u - c$ to remain positive, we set $\hat{c}_1 = -\overline{c}$ where $\overline{c} > 0$.

Outside the boundary layer, the solution can be written

[3] Solutions near the maximum of u are discussed later.

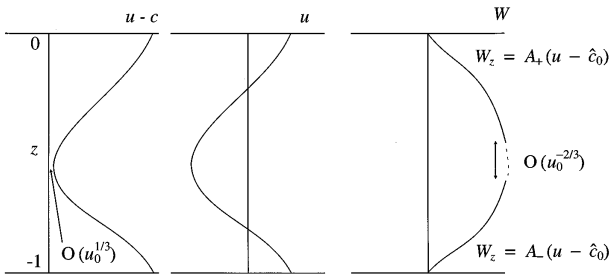

FIG. 2. Schematic of the large u case.

$$W = A_+ \int_{z_0}^{z} (u - u_{\min})\, dz + B_+, \qquad z > z_0$$

$$W = A_- \int_{z_0}^{z} (u - u_{\min})\, dz + B_-, \qquad z < z_0. \quad (29)$$

Here A_+, A_-, B_+, and B_- are unknown constants. Since the integrand is positive, we shall need A_+ and A_- to have opposite signs so that W_z will be one sign above $z = z_0$ and the other below it. Thus $W(z)$ will qualitatively resemble a first-mode solution; the boundary layer affects only high-order derivatives. Figure 2 shows a schematic.

The matching details are straightforward (see, e.g., Van Dyke 1975). To leading order the solution is a constant as it passes through z_0 (this is where W attains its single maximum), so that $B_- = B_+ = B$, say, some constant. To find out how A_- and A_+ are related, we integrate $(9)/(u - c)^2$ across $z = z_0$:

$$\left[\frac{W_z}{u - c}\right]_-^+ + N^2(z_0)B \int_-^+ dz \Big/ \left[\frac{1}{2}u_{zz}(z - z_0)^2 + \bar{c}\right]^2 = 0. \quad (30)$$

Here $+$, $-$ denote values of z just above and below z_0, respectively. The first term in (30) is just $(A_+ - A_-)$, and we use

$$\int_{-\infty}^{\infty} \frac{dx}{(x^2 + a^2)^2} = \frac{\pi}{2a^3} \quad (31)$$

to find

$$A_+ - A_- = -\frac{\pi N^2(z_0)B}{2^{1/2}u_{zz}^{1/2}\bar{c}^{3/2}}. \quad (32)$$

Now we apply the boundary conditions on W. These give

$$A_- = \frac{B}{\displaystyle\int_{-1}^{z_0} (u - u_{\min})\, dz};$$

$$A_+ = \frac{-B}{\displaystyle\int_{z_0}^{0} (u - u_{\min})\, dz}. \quad (33)$$

Use of (32) then gives

$$\frac{1}{\displaystyle\int_{-1}^{z_0} (u - u_{\min})\, dz} + \frac{1}{\displaystyle\int_{z_0}^{0} (u - u_{\min})\, dz} = \frac{\pi N^2(z_0)}{2^{1/2}u_{zz}^{1/2}\bar{c}^{3/2}} \quad (34)$$

so that, using $\int_{-1}^{0} u\, dz = 0$ by supposition,

$$\bar{c} = \left(\frac{\pi N^2(z_0)\left[\displaystyle\int_{-1}^{z_0} (u - u_{\min})\, dz\right]\left[\displaystyle\int_{z_0}^{0} (u - u_{\min})\, dz\right]}{|u_{\min}|}\right)^{2/3} \times \frac{1}{2^{1/3}u_{zz}^{1/3}} \propto u_0^{1/3} \quad (35)$$

and the phase speed c is then given by

$$c = u_{\min} - \bar{c}. \quad (36)$$

There is another, similar, solution situated near $u = u_{\max}$. In this case $c \approx u_{\max} + \bar{c}$, where now $\bar{c}$ is complex. The solution has

$$\bar{c} = \left(\frac{\pi N^2(z_0)\left[\displaystyle\int_{-1}^{z_0} (u - u_{\max})\, dz\right]\left[\displaystyle\int_{z_0}^{0} (u - u_{\max})\, dz\right]}{(-u_{\max})}\right)^{2/3} \times \frac{1}{2^{1/3}|u_{zz}|^{1/3}} \propto u_0^{1/3} e^{\pm 2i\pi/3}$$

since $u_{\max} > 0$. The solution has also been verified numerically. However, since the solution corresponds to an eastward propagating wave, it is of little use in describing anomalous westward propagation.

In summary, under these conditions, as the amplitude of the mean flow increases, there is always a mode whose phase speed is the most westward value of the mean flow, corrected westward by an amount that increases slowly with the amplitude of the mean flow. The solution (35) has been confirmed by direct integration in the asymptotic regime.

d. Summary

We have shown that in many circumstances, there is a mode, always resembling mode 1 in the vertical, whose phase speed is westward and usually faster than the mode 1 speed. In the case of mean flows that are small compared with the mode 1 phase velocity, the phase speed is the mode 1 speed adjusted by an amount proportional to the amplitude of the mean flow; this adjustment can have either sign in general. When the mean flow is as large as the mode 1 phase speed, the adjustment is now at least as large as the mode 1 speed. Dependent upon signs and distributions with depth, this adjustment can drive the eigenfunction more rapidly westward, or induce a critical layer and a (smaller) real

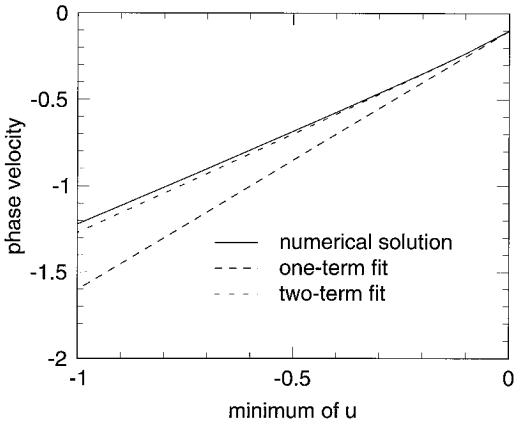

FIG. 3. Solutions for constant N, using a mode 2 u field. The firm line shows numerical solutions when the mid-depth minimum of u is westward (so u is eastward at the surface). The long-dashed line shows the one-term fit; the short-dashed line the two-term fit.

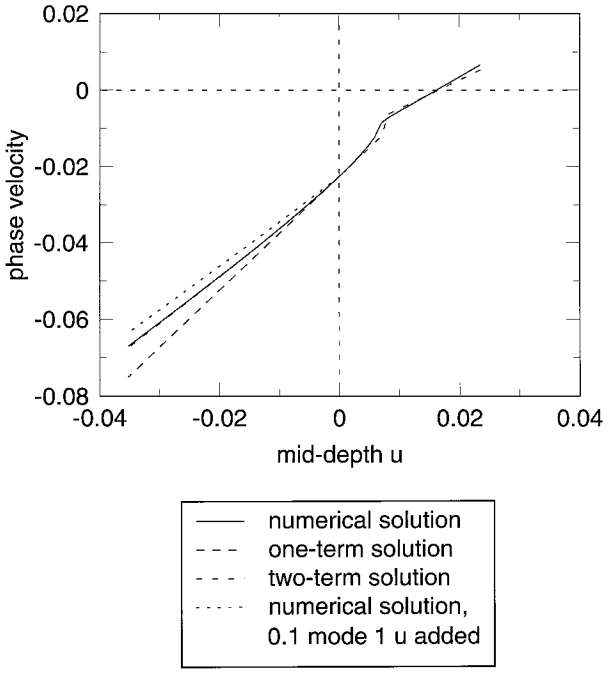

FIG. 4. Solutions for $N^2 = \exp 3.7z$, using a mode 2 u field. The x axis is the value of u at the mid-depth turning point (so negative values correspond to eastward surface flow, positive ones to westward surface flow). The firm line shows the numerical solution, which is complex to the right of the obvious bifurcation (beyond which only the real part of the phase velocity is shown). The long-dashed line shows the one-term solution (not drawn for positive mid-depth u for clarity). The short-dashed line the two-term solution, which is also plotted in where the numerical solution becomes complex. The dotted line shows the small change induced by adding some mode 1 u velocity in the negative mid-depth regime.

phase speed. When the mean flow is much larger than the mode 1 phase speed, then provided the maximum westward mean flow does not occur at the surface or the floor, there is a mode whose phase velocity is approximately the minimum value of the applied mean u field, modified westward by a further amount that increases as the strength of the mean flow increases.

These results will now be tested for some simple configurations in section 4.

4. Simple numerical examples

a. Uniform stratification

The simplest example sets $N = 1$ everywhere. This is not particularly physical, but permits easy analytical evaluation. Thus $\hat{h}_i(z) = 2^{1/2} \sin i\pi z$, $c_i = -1/(i^2\pi^2)$, and $\hat{u}_i = 2^{1/2} \cos i\pi z/i\pi$. This flow would satisfy the necessary conditions for instability when $u_0^2 > \frac{1}{2}$, but remains stable. There are certain symmetries that reduce the number of α coefficients when higher modes are included. In the case of driving by mode 2 u (recall that driving by mode 1 alone would have no effect), we have $\alpha_{211} = -\alpha_{121} = -2^{1/2}\pi$, and (22) implies the linear solution

$$c \approx c_1 - \frac{3}{2^{3/2}\pi} u_2. \tag{37}$$

The next higher approximation (26) is a quadratic for c as a function of u_2. If u_2 is rewritten as the minimum value attained by $u(z)$ (i.e., at $z = -0.5$), then the two solutions yield Fig. 3. The behavior of the solution for negative $u_{\min}$ is nearly linear. For positive $u_{\min}$, the solution eventually becomes complex and always possesses a phase velocity more eastward than the unperturbed phase speed. The one-term approximation is everywhere good, and the two-term approximation almost indistinguishable. Although not shown, the large u asymptotic fits the numerical solution extremely well once the amplitude of u reaches about 5.

For this u field, then, the westward phase speed is given to a good degree of approximation as $(c_1 + u_{\min})$ over a wide range of u amplitudes [and (36) shows that this continues into the large u regime]. Thus to achieve a doubling or trebling of the phase velocity merely needs a u velocity that is westward at depth respectively at the same speed as, or twice the speed of, the linear phase velocity. For typical linear speeds of a few centimeters per second, this is clearly easy to achieve.

b. Exponential stratification

A more realistic case is that where $N^2 = \exp kz$. Based on a realistic fit to the Levitus and Boyer (1994) and Levitus et al. (1994) North Atlantic data, $k = 3.7$. The linear normal modes are given by a combination of Bessel functions with the familiar skew toward the surface and resemble most calculations for actual ocean areas. The first mode has $c_1 = -0.02262$. Figure 4 shows the numerical and approximate solutions in this case, also for the second mode u forcing, again indicated by the amplitude of the mid-depth u field. When this is neg-

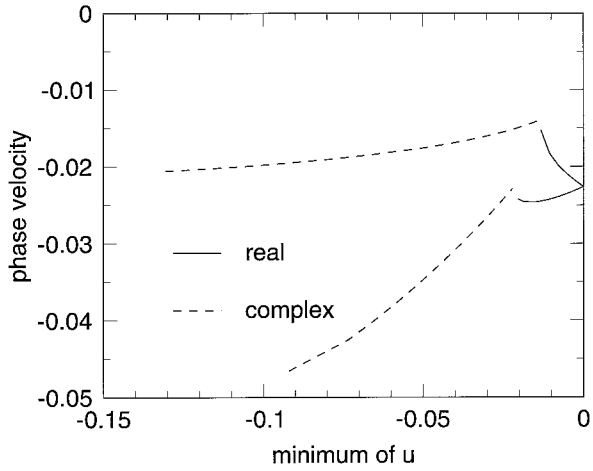

FIG. 5. Solutions for $N^2 = \exp 3.7z$ with $u = u_0(\exp z - 1 + e^{-1})$. There are two branches. The upper branch is where $u > 0$ at the surface, so u_{min} occurs at the floor. The lower branch is where $u < 0$ at the surface, where u_{min} is located. Both solutions become complex for values of u_{min} about the unperturbed phase speed. The upper branch continues beyond the end of plotting; the lower branch ceases to exist [$\mathrm{Im}(c) = 0$] beyond the end of the plotting.

ative, a similar picture emerges, with the phase speed varying roughly as $c_1 + u_{min}$. The one-term fit is excellent, and the two-term fit almost indistinguishable from the numerical solution. Also shown, for negative u_{min}, is the numerical solution when a mode 1 u field of amplitude 0.1 is added to the mean flow. As predicted earlier, there is very little change to the solution (which of course resembles the unperturbed mode 1 in shape).

To show that complex solutions do occur, the numerical solution is extended in the opposite direction (positive u_{min}). Beyond $u_{min} = 0.006$, there is a bifurcation and complex solutions set in; Fig. 4 shows the real part only. The solution stays fairly linear in u_{min} beyond the bifurcation, and the two-term fit remains excellent, as indicated.

c. An exponential u field

The two solutions above both display a quasi-linear behavior with u_{min}: as the mid-depth flow becomes larger and more negative, the phase speed increases westward at a rate roughly proportional to the applied u_{min} (and indeed would asymptote to precisely that value for large applied flows). This is not always the case, however. Consider the same stratification as (b) above, but replace the u field with

$$u = u_0(\exp(z) - 1 + e^{-1}). \tag{38}$$

(The additive constants ensure that u has no vertical integral.) The decay of u with depth is much slower than the decay of $N^2(z)$, so that it does not resemble a normal mode for this stratification. The necessary conditions for instability are satisfied only for $u_0 > -0.37$.

Figure 5 shows the phase velocity as u_0 is varied. There are two responses depending on whether u_0 is positive (upper branch) or negative (lower branch). Both solutions remain real only until u_{min} reaches values about the size of the unperturbed phase speed and then become complex. As the size of u_0 increases, the branch with positive surface u continues without difficulty; the branch with negative surface u ceases to exist where shown, and no solutions can be found. Because there is no interior turning point of u in this case, the large u asymptotic does not give a solution.

In both cases, however, values of u_{min} several times c_1 are needed before the westward phase speed is doubled, so that such a flow would be inefficient at increasing observed phase speeds. We must therefore expect that while the mechanism of interaction with the baroclinic flow can explain much of the increased phase speeds observed, it cannot explain all of them. The next section analyses the large-scale ocean circulation for evidence of the mechanism.

5. Local solutions in the ocean

The temperature–salinity data of Levitus and Boyer (1994) and Levitus et al. (1994) were analyzed to produce, on 1° squares, values of $N^2(z)$ and $u(z)$ at their standard depths. The former are not easy to do since the final horizontal smoothing in the data processing by Levitus et al. induces many inversions in the data. Cubic spline fits to temperature and salinity were used in the vertical, and then differentials of the spline structures in the vertical gave N^2 according to Gill's (1982) appendix; tests were also made using simple vertical differencing. Points where $N^2 < N^2_{crit} \equiv 2.5 \times 10^{-7}\ \mathrm{s}^{-2}$ had N^2 reset to N^2_{crit} to avoid difficulties. (N_{crit} is merely a device to avoid zero and negative values, and was chosen as a typical small value for the ocean.) There were many such points. Restricting attention to the latitude range $\pm$ (10 to 50)°, 74% of profiles had at least one point with very small N^2; using weighted vertical differencing reduced this percentage to 51%, but gave similar final answers. The spline fits were preferred on the grounds of smoothness. Not surprisingly, the profiles with small N^2 occurred preferentially toward the poles using either method of evaluation. However, most (53%) profiles with a small N^2 possessed only one such point. CDSNS discuss the calculation of deformation radii in more detail. We have used their approach to the ocean depth here: the depth was taken as the larger of the local depth and the depth in the Levitus data (i.e., the NODC standard depth), unless the former was more than 33% larger than the latter. This restriction was because when data are required below the last Levitus point, buoyancy frequency and velocity gradients must be copied downward. This extension of depths, as Chelton et al. note, can increase estimates of unperturbed phase speed by up to 10%.

The east–west velocity was deduced from thermal wind using in situ densities—that is, $fu_z = g\rho_y/\rho_0$. The

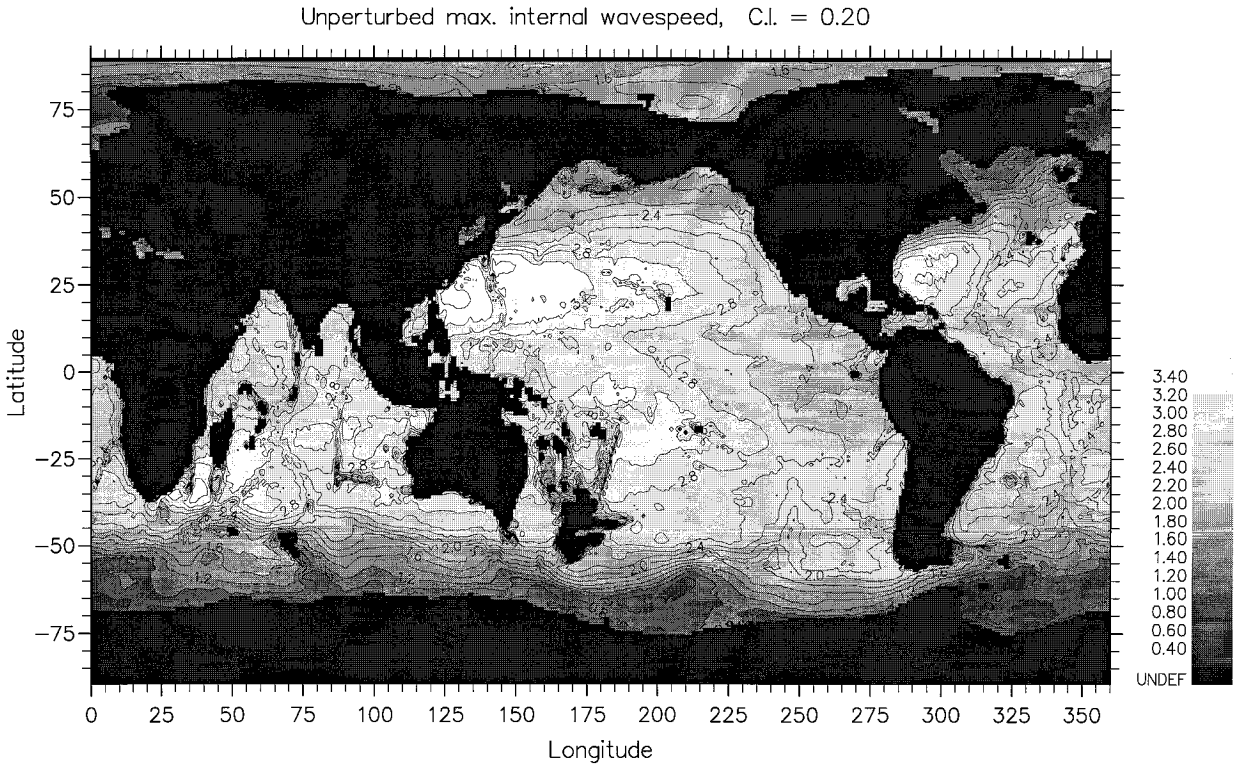

FIG. 6. The unperturbed mode 1 internal wave speed C_1 (in m s^{-1}) as computed from the Levitus and Boyer (1994) and Levitus et al. (1994) data. Contour interval 0.2 m s^{-1}.

northward derivative was computed using centered differences 1° north and south of the point under consideration.

The local depth H was thus taken as the minimum of the depth at the point in question and those 1°N and S so that u_z could meaningfully be defined everywhere. Points with depths less than 1000 m were treated as land. The baroclinic u field was then determined by subtracting the vertical average of u.

Both the linear wave problem (to deduce C_1 and c_1), and the wave problem with a nonzero $u(z)$ were solved in the same way. The eigenvalue problem (9) was posed as a vertical finite-difference eigenvalue problem of the form

$$\mathbf{AW} = c\mathbf{BW}, \tag{39}$$

where $\mathbf{W}$ represents a column vector at the standard depths in Levitus and Boyer (1994), and $\mathbf{A}$, $\mathbf{B}$ are matrices; c is the relevant eigenvalue. Because the original problem is not self-adjoint,[4] there is little convenient information about eigenvalues and vectors save only that if c is a complex eigenvalue, so is its complex conjugate. The matrix problem (39) normally produces $M - 2$ solutions if there are M points in the vertical; $M \leq 34$ by the prescribed choice of depths.[5] NAGLIB and other standard solvers were used for (39). Similar answers were found using a shooting method, although this tended to have more occurrences where no solution could be found.

For the linear (unperturbed) problem, all solutions exist and are oriented westward. Figure 6 shows the unperturbed first internal wave mode speed C_1 as a function of position (actually converted from the long planetary wave speed by $c_1 = -\beta C_1^2/f^2$). Its features are familiar: a gradual poleward decrease as top-to-bottom density contrasts shrink (plus an increase in areas of the Arctic due to the freshwater capping by river inflow); an increase in western basins compared with eastern; and clear evidence of topography such as midocean ridges (caused because the local depth, rather than some fixed value, has been used). The long planetary wave speed, which is plotted in Fig. 7, is much more zonal because of its domination by the variation of f and agrees extremely well with values used by CS for their comparison with observations. Values close to the equator, where equatorial Kelvin and planetary wave theory hold, are not shown.

[4] It can be made so, but only by making the problem nonlinear in c.

[5] Two of the solutions are null because they correspond to the boundary conditions $W = 0$ at top and bottom.

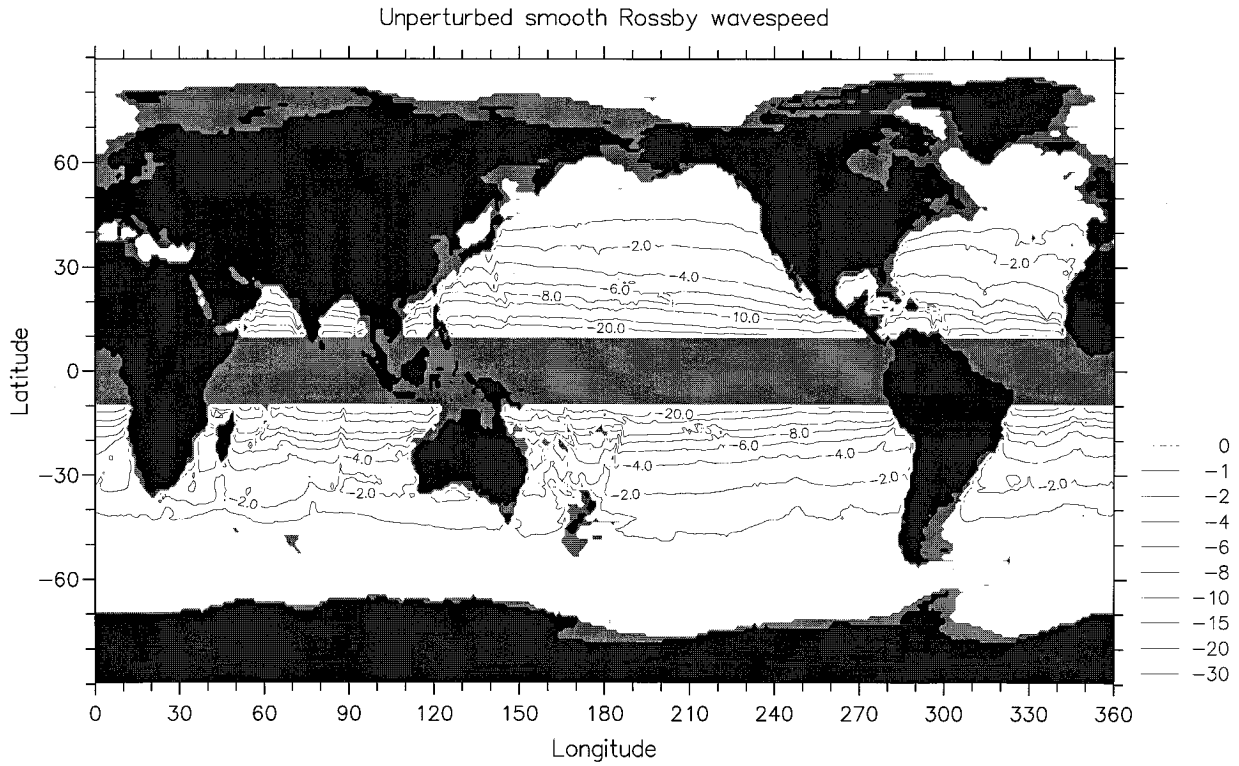

FIG. 7. The unperturbed fastest long planetary wave speed (in cm s^{-1}) (simply $-\beta/f^2$ times the square of the unperturbed internal wave speed shown in Fig. 6). Contour intervals are nonuniform: 30, 20, 15, 10, 8, 6, 4, 2, 1, and 0 cm s^{-1} westward. (The values 30 and 0 do not occur, but are added for comparison with later diagrams.) The values are masked within 10° of the equator, where equatorial, rather than long planetary wave, theory should hold.

We turn now to the problem with a baroclinic u field. The number of points with small N^2 values has a strong effect on the necessary conditions for instability, by inducing sign changes in the vertical derivative in q_y. All points in the latitude range ± (10 to 50)° satisfied the necessary conditions.

Figure 8 shows the zonally averaged minimum u velocity together with the unperturbed, linear westward phase speed. For latitudes below 20°, the assumption of a small perturbation from c is probably accurate, becoming less so for higher latitudes. In the Southern Ocean, the influence of the Antarctic Circumpolar Current (ACC) is evident, with baroclinic velocities far exceeding the linear phase speed. The effects of a mean flow should become proportionally stronger at higher latitudes, therefore. The magnitude of the effect will depend on the shape of the u field, as discussed earlier: if u is predominantly mode 1 in structure, then it is likely to have a small effect on the propagation speed, whereas if there is a significant mode 2 contribution, the phase speed should be modified.

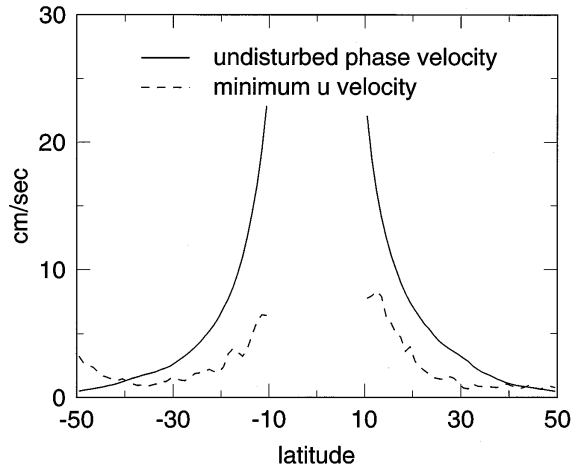

FIG. 8. Zonal averages of the unperturbed linear phase speed and the minimum baroclinic u velocity as functions of latitude.

Accordingly, Fig. 9 shows the percentage contribution of the local mode 2 u structure to the u field itself. In much of the ocean the first mode dominates the east–west flow; this is because the first mode has no sign changes in u_z and hence in ρ_y, which is to be expected since the majority of density gradients are of course poleward. The mode 2 contribution is dominant in latitudes of about 30°N or S, in bands of about 10° width, at the equatorward end of the subtropical gyres, since the flow here has the wrong sign of u_z at the surface.

Before presenting numerical solutions with a bar-

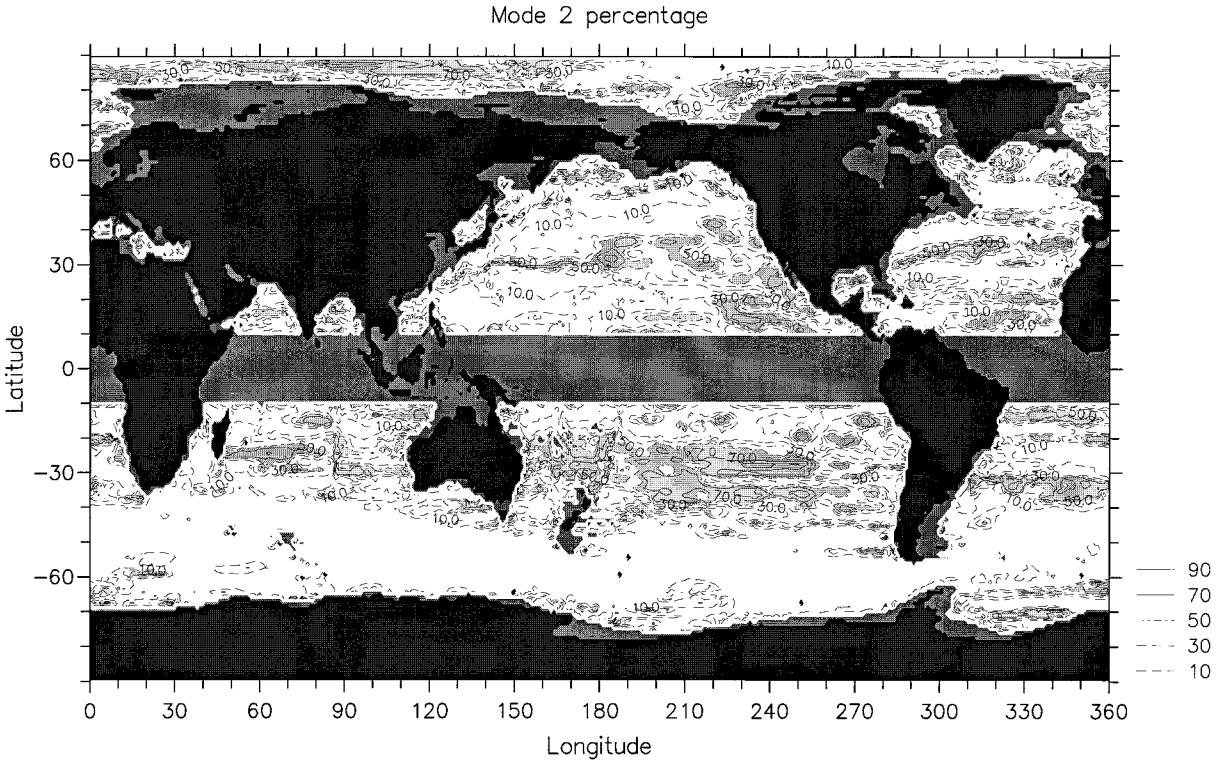

FIG. 9. The percentage of the baroclinic u field accounted for by the unperturbed internal second mode. Contours are drawn at 10%, 30%, 50%, 70%, and 90%; the shaded area denotes 50% and above.

oclinic u field, a problem of interpretation must be discussed. Since the continuous problems above have very few solutions, it follows that most, and sometimes all, of the $M - 2$ solutions produced will be false. This is a common problem with such methods, and the ''correct'' solution(s) must be chosen somehow. The best method of selection is by eye, but this is impractical at this resolution. Instead, several criteria were employed to select the correct solution. These were checked along one column of longitude, and the resulting eigenvalues scanned visually elsewhere. As a first test, we ensure that for a real solution, $c < u_{\min}$; for a complex solution, $c < u_{\max}$. Since most solutions have highly unphysical values of c, this is a good starting point. Two solutions were then selected: that with the least value of Re(c), that is, the one propagating westward fastest, and the solution that was smoothest in the vertical (using a norm involving the integral of $|W_{zz}|^2/|W|^2$). These two solutions were identical only in about half the locations, with the smooth solution preferentially having a very weak east–west phase speed. In what follows we present only the maximum westward velocity solutions.

In a very few locations—16 points in the range ± (10 to 50)°, or less than $\frac{1}{10}$% of the area, plus another 197 poleward of this range—the eigenvalue routine failed to produce *any* solutions that fit the above criteria. Examination of the eigenvalues showed that they were all real and lay consistently in the range $u_{\min} < c < u_{\max}$, with one eigenvalue lying in the range between two adjacent gridded u values. Since these would correspond to critical layers, they can be rejected.

Figure 10 shows the fastest westward mode. This was almost always (>90%) real in the latitude range ± (10° to 30°). There were small areas where the phase speed is positive (corresponding to *eastward* flow) in very high latitudes. Northward of 30° N more complex solutions occurred, reaching 60% of solutions at latitudes near 50°N, though on average between 30° and 50°N only about 14% of solutions were complex. South of 30°S, the proportion of complex solutions grows almost linearly with latitude, reaching 87% at 50°S. There are scattered points where the imaginary part of the phase velocity exceeded 1 cm s^{-1}. In most locations up to about ±40°, the solution was real. Southward of 40°S values the imaginary part rose to about 0.3 cm s^{-1}. As a guide, complex solutions (which are not shown) are found to a good degree of accuracy, where no contours of the mode-2 percentage are shown in Fig. 9. There were small areas where the phase speed is positive (corresponding to *eastward* flow) in very high latitudes.

Figure 10 has more structure than the predominantly zonally oriented Fig. 7. Values of c in the subtropics, as we shall see, are somewhat larger (10% to

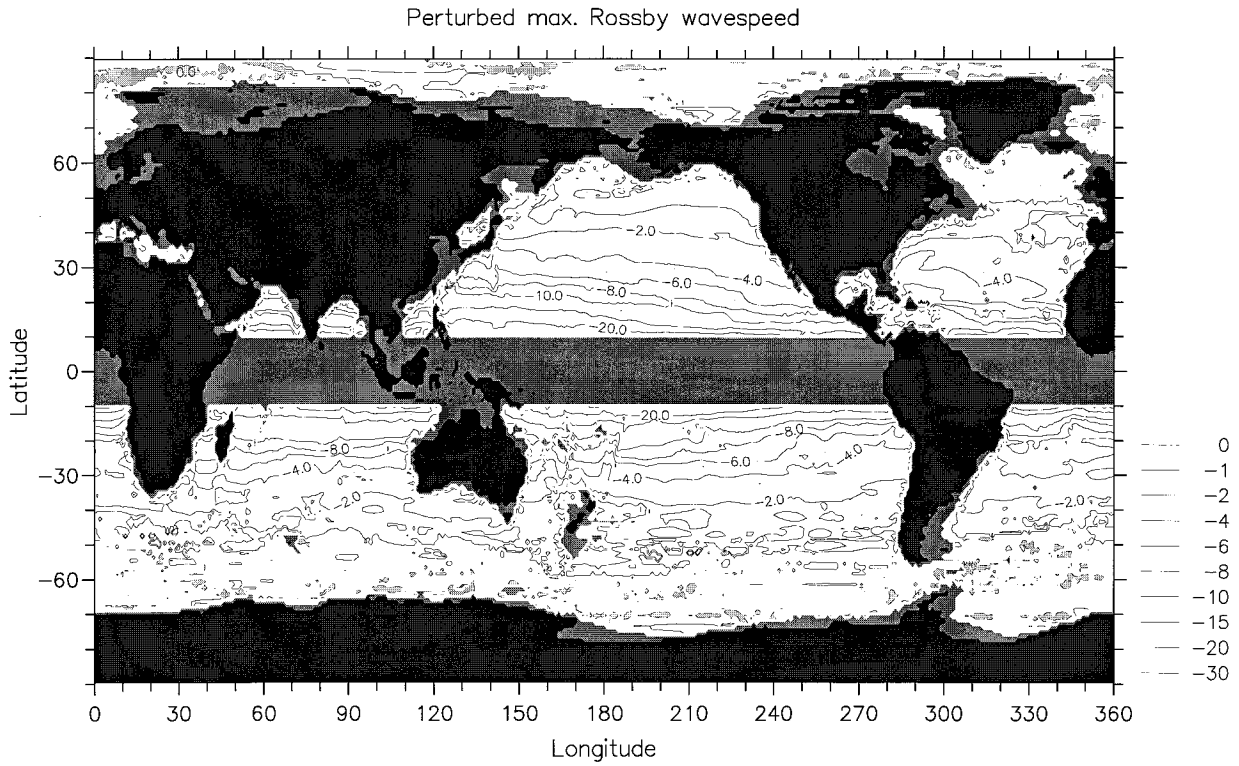

FIG. 10. The fastest long planetary wave speed (in cm s^{-1}) in the presence of a baroclinic u field. Contour intervals are nonuniform: 30, 20, 15, 10, 8, 6, 4, 2, 1 westward, and zero. The areas of positive speed are shaded in light gray; the areas where no solution could be found in dark gray.

30%) than corresponding values in unperturbed flow, but the ratio increases steadily poleward of these locations. Values of c of more than 1 cm s^{-1} are usually observed up to a latitude of 45°–50°. There is evidence of topographic effects, especially over midocean ridges (this is a purely local effect, of course; the theory assumes a flat bottom).

To compare the unperturbed and perturbed speeds, Fig. 11 shows the zonal mean of c_1, its 95% range of variability at that latitude, and the zonal mean of the

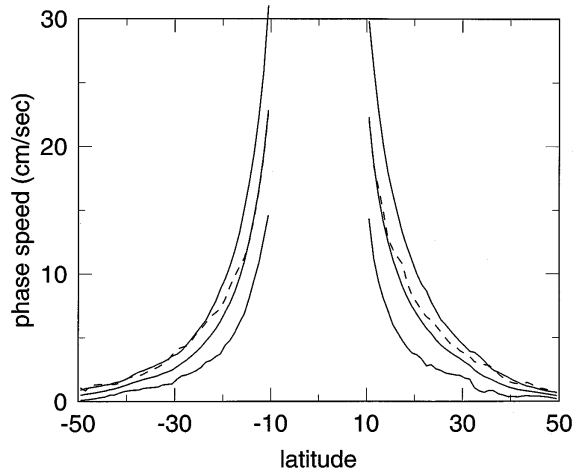

FIG. 11. The longitudinally averaged unperturbed long planetary wave speed, with 95% variability limits on either side (firm lines), and the fastest planetary wave speed with a baroclinic u field (dashed) as functions of latitude (in cm s^{-1}) (absolute values shown). Values near the equator are omitted.

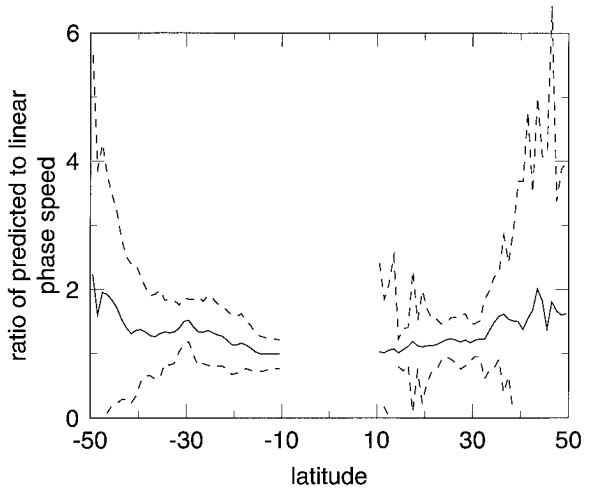

FIG. 12. The ratio of the long planetary wave speed with a baroclinic u field to that with no mean flow. The 95% variability interval on either side is also shown dashed; for clarity, the lower standard deviation is not plotted when it yields a negative value.

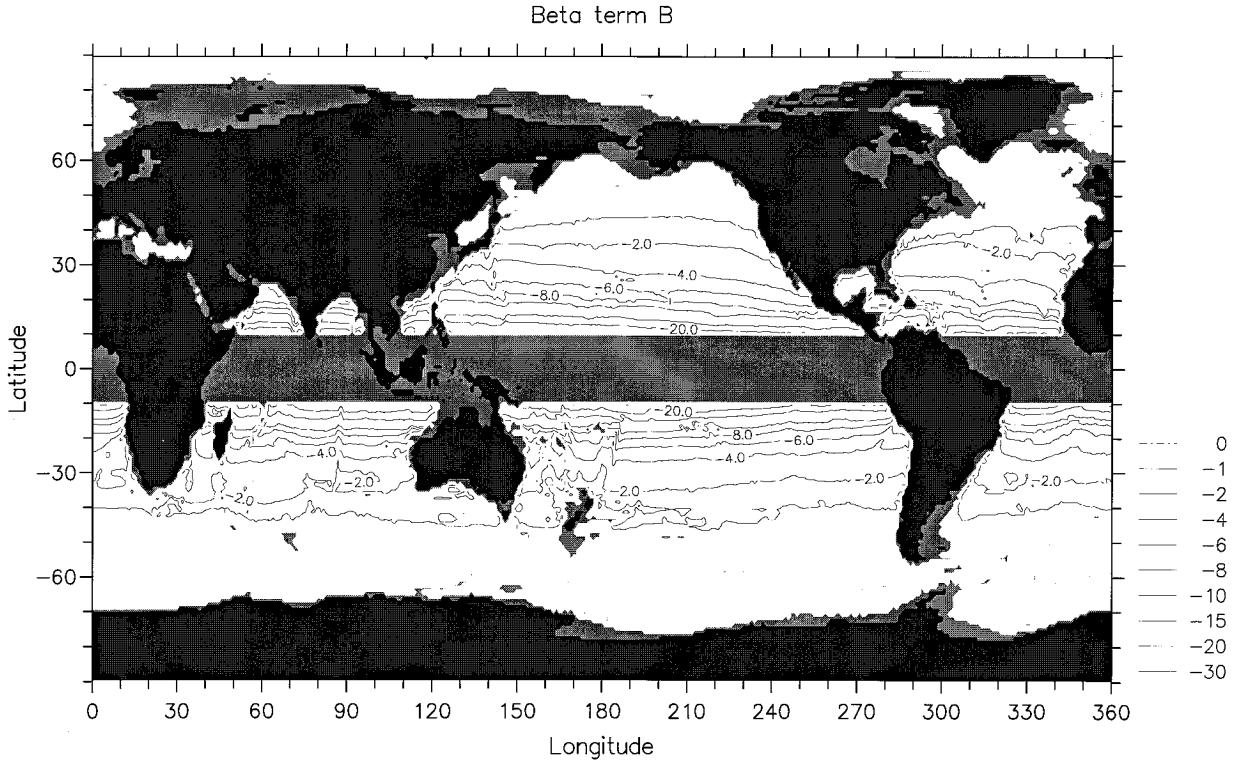

FIG. 13. Maps of the (a) beta, (b) steering, and (c) vortex stretching contributions to the planetary wave phase speed c for the perturbed case in dimensional form (cm s^{-1}).

fastest c in the presence of a baroclinic u field. The picture confirms the above observations. Poleward of 20°, the fastest c is at least one standard deviation faster than the unperturbed linear theory in both hemispheres, as observed. However, equatorward of 20° the perturbed speeds are within a standard deviation of what linear theory would suggest, which agrees with CS's data, although they show much scatter in this range. This diagram is in good agreement with the locations of the mode 2 contribution to the u field, with increases at 30° in both hemispheres, for example.

CS used specific longitude ranges, at a given latitude, for their comparisons. Figure 1b shows the ratios of observed to the perturbed phase speed in these ranges (the 95% variability range of these ratios was also computed but not shown for clarity). The results are mixed. In much of the Northern Hemisphere, the observations lie within the 95% limits; but between 30° and 40°S the theory still shows a strong underestimate. The observations still have a bias to faster speeds than predicted; of the 50 points shown, 52% of the speeds observed by CS lie outside the 95% confidence limits from the theory.

Figure 12 shows a more global comparison as a zonally averaged ratio. This ratio exceeds unity almost everywhere and increases poleward at most latitudes, attaining a ratio of 2 at 50°S. So the ratios remain somewhat smaller than those observed by CS, but there is a large zonal variation, as shown by the 95% variability limits, and the majority of CS's results fit within those limits easily. Thus the baroclinic model can account for most of the behavior of the observed ratios of planetary wave speeds given by CS.

6. A diagnostic interpretation of the perturbed phase speed

In this section we seek a simple explanation of the increase in phase speed, show a way to partition the various contributions of the earth's curvature (the beta effect) and baroclinic shear flow to the phase speed of planetary waves, and calculate and display these contributions in global maps. In particular, we will show some instructive examples of situations where the vertical structure of the shear flow and buoyancy frequency profile have led to markedly faster theoretical phase propagation speeds than the beta effect alone.

A measure of the integrated effect of shear flow on phase speed is derived by multiplying (7) by W^* and integrating from top to bottom. Using (10) we obtain

$$c = B + S + V, \tag{40}$$

where (retaining dimensionality for comparison with data below)

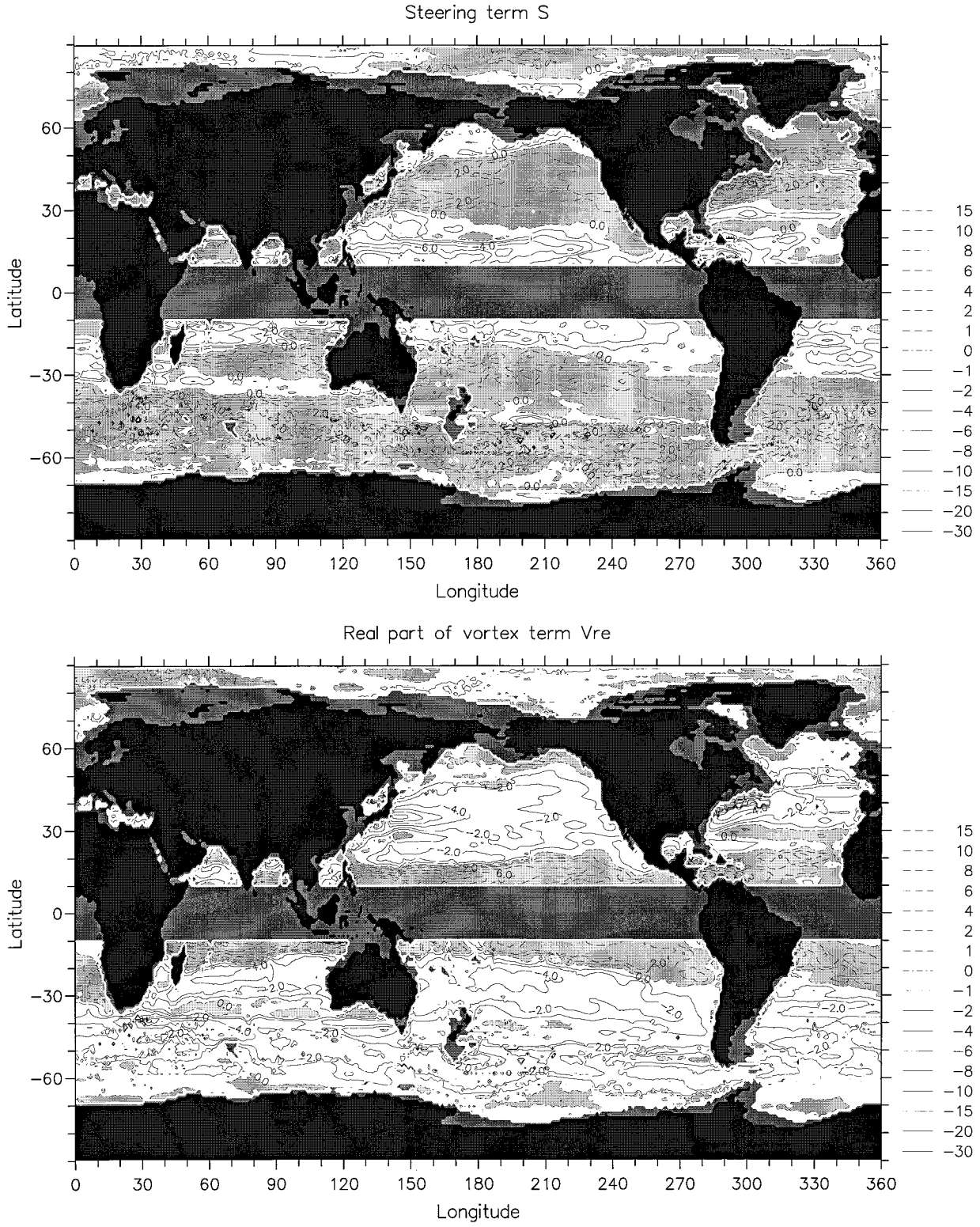

FIG. 13. *(Continued)*

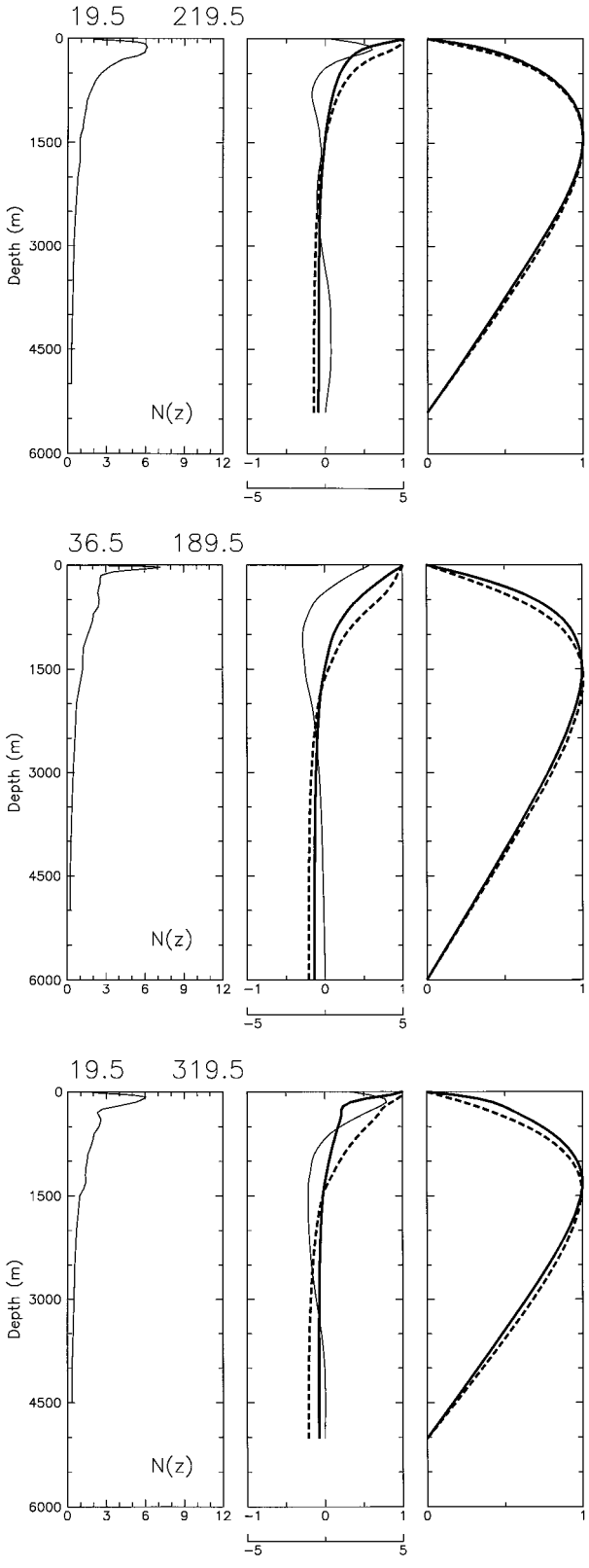

$$B = -\frac{1}{D}\frac{\beta}{f^2}\int_{-H}^{0} N^2|W|^2\,dz \quad \text{``beta term''} \tag{41a}$$

$$S = \frac{1}{D}\int_{-H}^{0} u|W_z|^2\,dz \quad \text{``steering term''} \tag{41b}$$

$$V = \frac{2}{D}\int_{-H}^{0} u_z W^* W_z\,dz \quad \text{``internal vortex stretching term''} \tag{41c}$$

$$D = \int_{-H}^{0} |W_z|^2\,dz. \tag{41d}$$

Because numerators and denominators are both quadratic in the wavefunction $W(z)$, none of the terms depends on the (arbitrary) amplitude chosen for the wavefunctions. The expression for the internal vortex stretching term is obtained from an integration by parts. The only possibly complex term is V.

It can be noted from (40) and (41) that the diagnostic expression for the phase speed in the unperturbed case $u(z) = 0$ reduces to choosing $W(z) = \hat{h}_1(z)$ and is

$$c_1 = -\frac{\beta}{f^2}\frac{\int_{-H}^{0} N^2\hat{h}_1^2\,dz}{\int_{-H}^{0} \hat{h}_{1z}^2\,dz}. \tag{42}$$

Figure 13 shows the (dimensional) contributions of the three terms of (40) to the total perturbed phase speed shown in Fig. 10. All three terms contribute significantly to the phase speed. It is remarkable that the beta term seldom differs from c_1 by more than 5% (cf. Fig. 13a with Fig. 7). Interesting and curious exceptions are narrow zonal bands across the North Atlantic at about 27°N and 20°N where B and c_1 differ by more than 10%. These features become very clear from a map of the ratio B/c_1 (not shown). A remarkable feature of the solutions of (7) is how little the forms of the vertical velocity wavefunctions $W(z)$ are altered by the addition of mean shear. Examples of wavefunction profiles of $W(z)$—in real cases—are shown by the heavy solid lines in the right panels of Fig. 14; the wavefunctions $\hat{h}_1(z)$ for the unperturbed case are shown by the heavy dashed lines. The similarity between $W(z)$ and $\hat{h}_1$ explains the general close similarity of B and c_1 as given by (41a) and (42), respectively.

←

FIG. 14. Example vertical profiles of $N(z)$, $u(z)$, and the wavefunctions for the perturbed and unperturbed cases at locations (a) 19.5°N, 219.5°E; (b) 19.5°N, 319.5°E; and (c) 36.5°N, 189.5°E. Left panels: $N(z)$. Middle Panels: $u(z)$ (thin solid lines), $W_z(z)$ (heavy solid lines), and $\hat{h}_{1z}(z)$ (heavy dashed lines). Right panels: $W(z)$ (heavy solid lines) and $\hat{h}_1(z)$ (heavy dashed lines). Relevant quantities are (in cm s^{-1}) (a) $c_1 = -8.08$, $c = -7.72$, $B = -7.78$, $S = -1.35$, $V = 1.41$; (b) $c_1 = -2.06$, $c = -3.66$, $B = -1.99$, $S = 1.32$, $V = -2.99$; (c) $c_1 = -6.66$, $c = -6.69$, $B = -5.63$, $S = -2.35$, $V = 1.29$.

The augmentation of c in the perturbed case is caused by the steering and vortex stretching terms, which are seen in Fig. 13 almost always to be in opposition. If u is proportional to W_z, these terms exactly cancel. (The wavefunctions $W_z = P$ are shown in the middle panels of Fig. 14.) This reflects the noninteraction result commented on in section 2. More generally, these terms in (40) can be combined into

$$\Delta c = S + V = -\frac{1}{D}\int_{-H}^{0} u[|W_z|^2 + 2W^*W_{zz}]\,dz$$

$$= \frac{1}{D}\int_{-H}^{0} u[-\partial_z^2(W^2) + W_z^2]\,dz \quad \text{if } W \text{ is real.} \quad (43)$$

This expression extracts the part of u that can cause shifts in the phase speed from c_1.

In midlatitudes in all ocean basins the vortex stretching term (41c) shown in Fig. 13c makes a westward contribution to c that prevails over the steering term (41b) shown in Fig. 13b by an amount comparable in magnitude to the beta term (invariably westward, of course). In the western section of the midlatitude North Pacific, for example, the ratio of total perturbed c to c_1 is as large as 2.0. Qualitatively, one may observe that in the northern limbs of the subtropical gyres and the southern limbs of the subarctic gyres the (surface) flow is eastward, giving positive steering terms. In these same regions, the mean geostrophic shear u_z is positive and proportional to isopycnal slope, which tends to increase toward the surface. Thus, $u_{zz} > 0$ (see examples in Fig. 14), giving a negative sign for the vortex stretching term (41c). In low latitudes where the mean circulation is westward, both terms tend to reverse sign, though individually and in sum they are a small proportion of the beta term. As a result, the phase speeds differ little from the unperturbed case at low latitudes. In a few regions, such as the southwestern region of the subtropical gyre of the North Pacific along 20°N, the steering and vortex stretching are the same sign though they are small compared to the beta term and therefore have little effect on the phase speed.

The three example profiles shown in Fig. 14 illustrate the range of effects that the shear profile can have on c. In Fig. 14a from the eastern subtropical North Pacific, $W(z)$ and $\hat{h}_1(z)$ are almost indistinguishable and B differs from c_1 by less than 4%. The S and V terms in (40) almost exactly cancel, resulting in no significant difference between c and c_1. In Fig. 14b from the midlatitude central North Pacific, the $W(z)$ and $\hat{h}_1(z)$ profiles are measurably different but still generally similar and B and c_1 again differ by less than 4%. In this case, however, the shear profile yields a V term more than twice the magnitude of the S term, resulting in $c/c_1 = 1.78$.

The third example shown in Fig. 14c is an exception to the general close agreement between B and c_1. This profile is from one of the subtropical bands in the North Atlantic in which it was noted above that B and c_1 differ by more than 10%. In this case, S and V differ by the same amount as B and c_1. The net result is that B, S, and V conspire in such a way that $c/c_1 = 1$.

The general similarity of the perturbed and unperturbed vertical velocity wavefunctions suggests a way to approximate (43). The unperturbed wavefunction $\hat{h}_1(z)$ very closely resembles the WKBJ form for the first baroclinic mode (CDSNS). Hence the perturbed wavefunction $W(z)$ may be approximated in the real case (ignoring normalization) by

$$W(z) \approx W_{\text{WKBJ}} = [\phi_1']^{-1/2}\sin\phi_1(z), \quad (44)$$

where

$$\phi_1(z) = \int_{-H}^{z}\left(\frac{\beta}{-c_1}\right)^{1/2} f^{-1}N(z')\,dz' \quad (45)$$

subject to $\phi_1(0) = \pi$ (which defines c_1). Then it is easy to confirm that, in the WKBJ approximation,

$$B = c_1 = -\frac{\beta}{\pi^2 f^2}\left(\int_{-H}^{0} N(z)\,dz\right)^2. \quad (46)$$

Using the approximation (44), it can be shown that

$$\frac{1}{D}[-\partial_z^2(W^2) + W_z^2] \approx \pi^{-1}\phi_1'(1 - 3\cos[2\phi_1(z)]). \quad (47)$$

Let

$$u = a_1W_z + a_2\cos[2\phi_1(z)]. \quad (48)$$

Then, from (46) and (47),

$$\Delta c \approx -\frac{3}{2}a_2. \quad (49)$$

This analysis will, of course, fail if Δc becomes large and positive enough to induce a critical layer.

The WKBJ analysis thus reveals that it is the part of $u(z)$ proportional to the second *unperturbed* WKBJ mode that causes the increased phase speed in the perturbed case. Contributions $a_n\cos[n\phi(z)]$ to $u(z)$ from higher-order WKBJ modes can be shown to contribute almost nothing to Δc defined by (43).

Another way to see this effect is to assume $W_1 \gg W_j$, $j > 1$ in (19). Thus, neglecting the j sum, setting $k = 1$, and neglecting contributions to u from modes higher than 2, (19) can be written

$$\Delta c = u_2c_1\left(\alpha_{121} - \alpha_{211}\frac{c_2}{c_1}\right),$$

showing again that the change in c is generated by the amount of second mode u field present.

Yet further confirmation of this approach is found by recomputing the solutions using as an east–west flow either the baroclinic u field with the mode 1 contribution removed, or only the mode 2 contribution to the baroclinic u field. The westward phase speeds are extremely

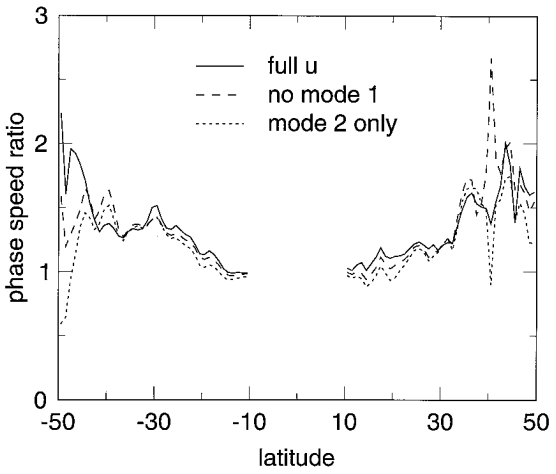

FIG. 15. A comparison of the predicted phase speed ratios using the full u field (firm line), the u field with its mode 1 contribution removed (dashed line), and the mode 2 contribution only of the u field (dotted line).

similar to those using the full u field (and are not shown). As a summary, Fig. 15 shows the longitudinal-averaged ratio of phase speed to the unperturbed case from the original calculation and the two just mentioned. Overall, the three results are similar apart from some noise at high latitudes. Over midlatitudes, there is a consistent decrease in ratio from the original calculation (highest), through the no mode 1 case, to a smallest value for the mode 2 calculation alone; but this reduction is small, of order 10%. This again demonstrates the importance of the mode 2 u field.

In conclusion, it is apparent from the partitioning of the phase speeds of perturbed planetary waves by the diagnostic equation (40) and (41) that the background mean shear flow can significantly alter the phase speed. At middle and high latitudes, the steering and vortex stretching contributions combine to yield net westward phase speeds systematically higher than those obtained from the unperturbed case. The portion of $u(z)$ proportional to the second unperturbed baroclinic mode is responsible for the increased phase speeds.

7. Effects of the mean barotropic field

We have seen that the mechanism of modes within a baroclinic u field can explain much but not all of the observed planetary wave speeds. However, barotropic flows in the ocean, although they are believed to be small, could have an effect. Since this is purely a Doppler shift, the effect should be easy to estimate, given adequate data. Estimates of barotropic flow are almost nonexistent from observations. Eddy-admitting ocean models compute barotropic as well as baroclinic flow. Two models are used here.

Semtner and Chervin's (1992) quasi-global eddy-admitting model contains plausible values for depth-integrated streamfunction, from which estimates of barotropic east–west flow can be obtained (10×10^6 m^3 s^{-1} flux in 10° of latitude in a depth of 5000 m is a mean flow of 0.2 cm s^{-1}). The strongest flows, apart from western boundary currents, which contribute little to the global estimates earlier, lie in the ACC (which is partly outside the region of interest here anyway). They report a flux of 200×10^6 m^3 s^{-1} over 20° of latitude, corresponding to 2.3 cm s^{-1} eastward barotropic flow. This reduces the very large ratios observed at 50°S, but they remain much larger than unity. A more ''normal'' value would be the flow in the region 10°–30°N in the subtropical gyre, where the predicted speeds are too small. Semtner and Chervin show a flux of 60×10^6 m^3 s^{-1} over 20° of latitude, corresponding to 0.7 cm s^{-1} westward barotropic flow. While small, this is enough to increase ratios of predicted to unperturbed wave speeds over most of the region.

More quantitative calculations can be made using OCCAM (Ocean Circulation and Climate Advanced Modelling) output (Gwilliam et al. 1997). This free-surface global model has a resolution of ¼°, and the data used here are time averages over years 5–7 of the run. The barotropic east–west velocity was extracted and simply added to the predicted c values, as well as the baroclinic u velocity. All relevant statistics were then recomputed using these revised values.

The OCCAM barotropic velocities (not shown) are noticeably stronger in many regions than was estimated from the Semtner and Chervin streamfunction, as well as being noisier (although the noise is well resolved within the numerical model, and is mostly related to strong narrow jets and stationary eddies). Many regions of strong flow exist in shallow regions, of course, as well as boundary current extensions and ACC flow; the majority of these strong flows are eastward. Some 33% of the ocean area indicated in Fig. 10 has barotropic east–west flow above 1 cm s^{-1} in magnitude.

Figure 16 shows the phase velocities with the barotropic flow added, that is, the equivalent of Fig. 10. The effects of the strong eastward barotropic flows in the ACC and western boundary current extensions are clearly visible and are strong enough to advect the planetary waves eastward. This gives rise to numerous interesting features involving the interactions of planetary waves with critical layers, which are discussed by Hughes (1995). The spatial variability makes it hard to see immediately whether inclusion of the barotropic flow has improved or deteriorated the agreement with data. Perhaps surprisingly, there is little change over much of the ocean to many of the statistics. For example, the zonally averaged minimum u velocity only differs noticeably in the region south of 40°S, where it becomes very small. The zonally averaged phase speed, including the barotropic flow, is also little changed save, again, south of 40°S where it too becomes eastward. The ratios of observed to predicted phase speed are now much noisier than previously, with very large longitudinal

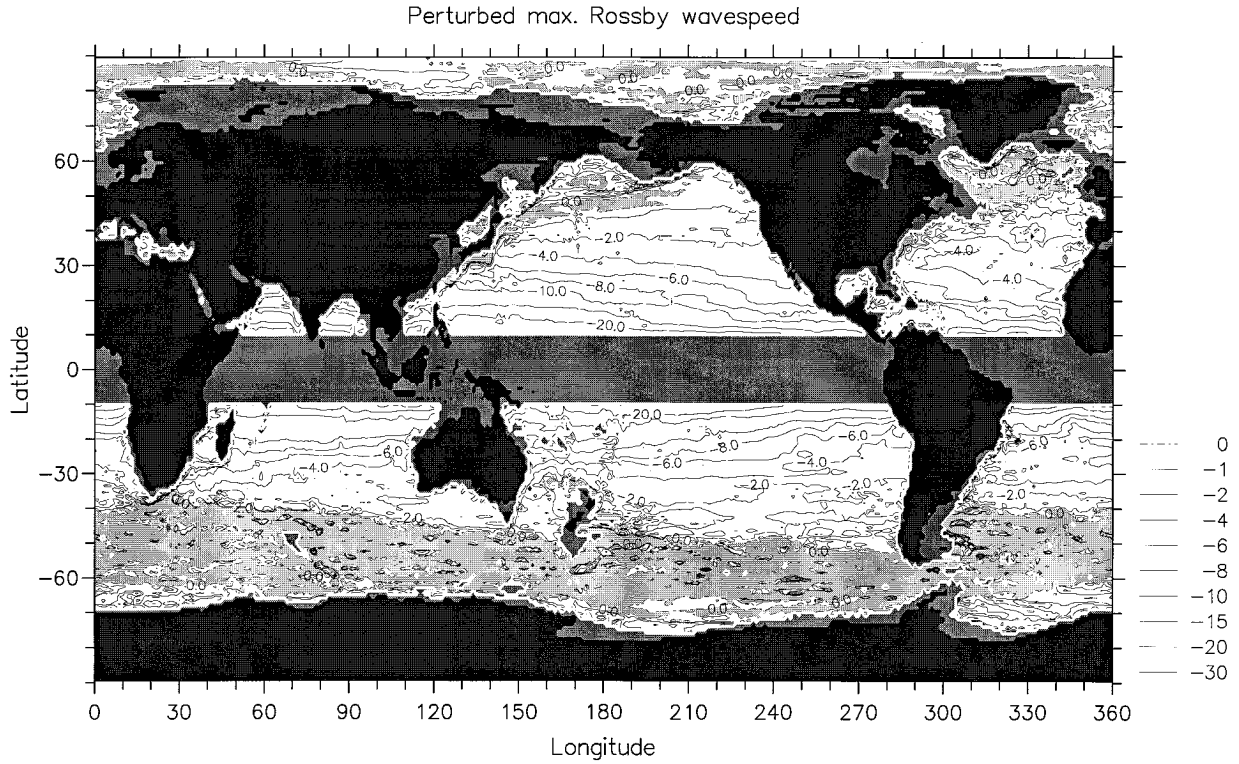

FIG. 16. The fastest long planetary wave speed (in cm s^{-1}) in the presence of a baroclinic and barotropic *u* field (the latter from the OCCAM model). Details as for Fig. 10.

variability poleward of 30° (and indeed, almost any observed ratio would lie within 95% variability limits).

A better test is to repeat the specific calculations at the locations used by CS (as in Fig. 1b); the results are shown in Fig. 1c. Whether the fit with data is improved is equivocal. Statistically, fewer (44%) of the points now lie outside the 95% variability limits. This is due to two reasons: the predicted speeds are almost everywhere increased from the pure baroclinic theory and the increased variability has increased the standard deviations around a latitude band and, thus, widened the confidence limits. The fit is probably improved between 30° and 40°S but worsened at 50°S since the barotropic flow begins to feel the (eastward) ACC.

The inclusion of barotropic flow thus appears to have small, and mixed, effects on the model fit to observations.

8. Conclusions

This paper has asked a single question: why is there a discrepancy (toward higher values) between observed and theoretical long planetary waves? Of various possibilities, it was concluded that changes in the potential vorticity gradient induced by the presence of mean flow was most likely to alter the linear theory. Attention was concentrated on baroclinic flows. A set of simple problems were solved approximately for east–west mean flows, showing that wave propagation could be much more rapid in the presence of such flows. The problem was then solved globally using archive temperature–salinity data, and the majority of observed speed ratios produced by the theory. Inclusion of numerical model predictions of barotropic flow does not have a strong effect on the fit to data. The change in phase speed is mostly accounted for by (unperturbed) mode 2 east–west velocity; mode 1 velocity was shown to have almost no effect on wave propagation. Although other mechanisms will inevitably be involved in a complete theory for planetary wave propagation, the mechanism in this paper *must* be included since the waves respond to the total potential vorticity gradient.

The model has implicitly assumed that the background *u* field does not change as the wave propagates, whereas the data demonstrate that this is not the case. Thus, the wave properties must be gradually modified (producing scattering and refraction problems) during westward propagation. Such a problem is beyond the scope of this work; we can merely note here that, since the vertical structure of the fastest mode is first-mode-like everywhere, the scattering is likely to be small so that propagation will not be strongly affected.

Similarly, the model explicitly ignored mean flows in other directions because such mean flows would be intrinsically three-dimensional in nature. In addition, pure east–west propagation is not affected by north–south

mean flow. However, it is possible that the propagation is not oriented exactly east–west. As a test, the mean flow was modified as in (6) to include the north–south flow, and propagation at an angle $\pm 10°$ north or south of westward was examined. The changes were everywhere tiny, being about 3% at maximum. A further change to $\pm 45°$ also yielded only small changes. Thus, realistic changes in propagation direction do not affect the calculation.

Nonetheless, a natural extension to the work would be to take a coherent three-dimensional velocity field (e.g., a long-term average of a general circulation model) and propagate the planetary geostrophic equations through that field as a small perturbation, identifying wave speeds either by time–space diagrams and Radon transforms (CS or Cipollini et al. 1996) or by Fourier decomposition (Cipollini et al. 1997).

Acknowledgments. Our thanks to Jeff Blundell and Michael Schlax for computing the solutions in sections 5 and 6. It is a pleasure to record the enthusiasm demonstrated by the satellite team at SOC during this work. This research was supported by Contract 958127 from the Jet Propulsion Laboratory funded under the TOPEX/POSEIDON Announcement of Opportunity, by Grant NAGW-3051 from the National Aeronautics and Space Administration, and by Grant OCE-9402891 from the National Science Foundation.

REFERENCES

Anderson, D. L. T., and P. D. Killworth, 1977: Spin-up of a stratified ocean with topography. *Deep-Sea Res.*, **24,** 709–732.

——, and ——, 1979: Nonlinear propagation of long internal Rossby waves. *Deep-Sea Res.*, **26,** 1033–1050.

Beckmann, A., C. W. Böning, B. Brügge, and D. Stammer, 1994: On the generation and role of eddy variability in the central North Atlantic Ocean. *J. Geophys. Res.*, **99,** 20 381–20 391.

Chang, P., and S. G. H. Philander, 1989: Rossby wave packets in baroclinic mean currents. *Deep-Sea Res.*, **36,** 17–37.

Charney, J. G., and M. E. Stern, 1962: On the stability of internal baroclinic jets in a rotating atmosphere. *J. Atmos. Sci.*, **19,** 159–172.

Chelton, D. B., and M. G. Schlax, 1996: Global observations of oceanic Rossby waves. *Science,* **272,** 234–238.

——, R. A. de Szoeke, M. G. Schlax, K. E. Naggar, and N. Siwertz, 1997: Geographical variability of the first baroclinic Rossby radius of deformation. *J. Phys. Oceanogr.*, in press.

Cipollini, P., D. Cromwell, and G. D. Quartly, 1996: Variability of Rossby wave propagation in the North Atlantic from TOPEX/POSEIDON altimetry. *Proc. IEEE Intl. Geoscience and Remote Sensing Symp. (IGARSS '96),* Lincoln, NE, IEEE, 91–93.

——, ——, and ——, 1997: Observations of Rossby wave propagation in the Northeast Atlantic with TOPEX/POSEIDON altimetry. *Adv. Space Res.*, in press.

Clarke, A. J., 1982: Dynamics of large-scale wind-driven variations in the Antarctic Circumpolar Current. *J. Phys. Oceanogr.*, **12,** 1092–1105.

Dickinson, R. E., 1978: Rossby waves—Long-period oscillations of oceans and atmospheres. *Annu. Rev. Fluid Mech.*, **10,** 159–195.

Forbes, C., K. Leaman, D. Olson, and O. Brown, 1993: Eddy and wave dynamics in the South Atlantic as diagnosed from Geosat altimeter data. *J. Geophys. Res.*, **98,** 12 297–12 314.

Gill, A. E., 1982: *Atmosphere-Ocean Dynamics.* Academic Press, 662 pp.

——, J. S. A. Green, and A. J. Simmons, 1974: Energy partition in the large-scale ocean circulation and the production of mid-ocean eddies. *Deep-Sea. Res.*, **21,** 499–528.

Glazman, R. E., A. Fabrikant, and A. Greysukh, 1996: Statistics of spatial-temporal variations of sea surface height based on TOPEX altimeter measurements. *Int. J. Remote Sens.*, **17,** 2647–2666.

Gwilliam, C. S., A. C. Coward, B. A. de Cuevas, D. J. Webb, E. Rourke, S. R. Thompson, and K. Döös, 1997: The OCCAM global ocean model. *Proc. Second UNAM-Cray Supercomputing Conf.: Numerical Simulations in the Environmental and Earth Sciences,* Mexico City, Mexico, Cray Research, in press.

Held, I. M., 1983: Stationary and quasi-stationary eddies in the extratropical troposphere: Theory. *Large-Scale Dynamical Processes in the Atmosphere,* B. J. Hoskins, and R. P. Pearce, Eds., Academic Press, 127–168.

Herrmann, P., and W. Krauss, 1989: Generation and propagation of annual Rossby waves in the North Atlantic. *J. Phys. Oceanogr.*, **19,** 727–744.

Hughes, C. W., 1995: Rossby waves in the Southern Ocean: A comparison of TOPEX/POSEIDON altimetry with model predictions. *J. Geophys. Res.*, **100,** 15 933–15 950.

Jacobs, G. A., H. E. Hurlburt, J. C. Kindle, E. J. Metzger, J. L. Mitchell, W. J. Teague, and A. J. Wallcraft, 1994: Decade-scale trans-Pacific propagation and warming effects of an El Niño anomaly. *Nature,* **370,** 360–363.

Kessler, W. S., 1990: Observations of long Rossby waves in the northern tropical Pacific. *J. Geophys. Res.*, **95,** 5183–5217.

Killworth, P. D., 1979: On the propagation of stable baroclinic Rossby waves through a mean shear flow. *Deep-Sea Res.*, **26,** 997–1031.

——, 1980: Barotropic and baroclinic instability in rotating stratified fluids. *Dyn. Atmos. Ocean.*, **4,** 143–184.

——, and D. L. T. Anderson, 1977: Meaningless modes? *Mode Hot-Line News* (unpublished manuscript), No. 72.

LeBlond, P. H., and L. A. Mysak, 1978: *Waves in the Ocean.* Elsevier, 602 pp.

Le Traon, P. Y., and J.-F. Minster, 1993: Sea level variability and semiannual Rossby waves in the south Atlantic subtropical gyre. *J. Geophys. Res.*, **98,** 12 315–12 326.

Levitus, S., and T. Boyer, 1994: *World Ocean Atlas 1994,* Vol 4: *Temperature,* NOAA Atlas NESDIS 4, U.S. Govt. Printing Office, 150 pp.

——, R. Burgett, and T. Boyer, 1994: *World Ocean Atlas 1994,* Vol 3: *Salinity,* NOAA Atlas NESDIS 3, U.S. Govt. Printing Office, 150 pp.

Meyers, G., 1979: On the annual Rossby wave in the tropical North Pacific Ocean. *J. Phys. Oceanogr.*, **9,** 663–674.

Pedlosky, J., 1964: An initial value problem in the theory of baroclinic instability. *Tellus,* **16,** 12–17.

——, 1987: *Geophysical Fluid Dynamics.* 2d ed. Springer Verlag, 710 pp.

Rhines, P. B., 1970: Edge-, bottom-, and Rossby waves in a rotating stratified fluid. *Geophys. Fluid Dyn.*, **1,** 273–302.

Rogel, P, J.-F. Minster, E. Blayo, J.-M. Molines, and J. Verron, 1996: Propagation of the dominant sea level signals in the North Atlantic from TOPEX-POSEIDON altimeter data. *J. Geophys. Res.*, in press.

Schopf, P., D. L. T. Anderson, and R. Smith, 1981: Beta-dispersion of low frequency Rossby waves. *Dyn. Atmos. Ocean.*, **5,** 187–214.

Semtner, A. J., and R. M. Chervin, 1992: Ocean general circulation from a global eddy-resolving model. *J. Geophys. Res.*, **97,** 5493–5550.

Welander, P., 1959: An advective model of the ocean thermocline. *Tellus,* **11,** 309–318.

White, W. B., 1977: Annual forcing of baroclinic long waves in the tropical North Pacific. *J. Phys. Oceanogr.*, **7,** 50–61.

——, 1985: The resonant response of interannual baroclinic Rossby waves to wind forcing in the eastern midlatitude North Pacific. *J. Phys. Oceanogr.*, **15,** 403–415.

Van Dyke, M., 1975: *Perturbation Methods in Fluid Mechanics.* Parabolic, 271 pp.